INFLUENCE OF AXIAL SPACING ON SPANWISE

EFFICIENCY OF A TRANSONIC AXIAL

COMPRESSOR ROTOR STAGE

By

MARK WILLIS DAVEY

Bachelor of Science

Oklahoma State University

Stillwater, Oklahoma State University

2002

INFLUENCE OF AXIAL SPACING ON SPANWISE

EFFICIENCY OF A TRANSONIC AXIAL

COMPRESSOR ROTOR STAGE

Thesis Approved:

David G Lilley
Thesis Advisor

Peter M Moretti

Andrew S Arena

Gordon Emslie
Dean of the Graduate College

ACKNOWLEDGEMENTS

I would like to thank my parents for their support during this venture. Without them I would not have been able to complete this endeavor.

I thank Dr. Eric Falk for providing me with this research opportunity. I appreciate the advice and direction he has given.

I would also like to thank Dr. Steven Gorrell who provided the opportunity and funding for this study.

I appreciate the guidance and advice that Dr. David Lilley provided on finishing my research and thesis. I would not have completed this study in the time I desired without him pushing me.

TABLE OF CONTENTS

LIST OF TABLES

LIST OF FIGURES

NOMENCLATURE

Symbols

V_{jet}	Velocity of tip clearance flow
V_{wall}	Velocity of V_{jet} and V_{wall}
VD	Velocity Difference
γ	Specific heats ratio, Angle between tip clearance flow and
η	Efficiency
π	Pressure Ratio
τ	Temperature Ratio

Acronyms

APG	Average Passage Grid
APNASA	Average Passage code developed by NASA
CARL	Compressor Aero Research Lab
ICOMP	Institute for Computational Mechanics in Propulsion
IGV	Inlet Guide Vane
SMI	Stage Matching Investigation
WG	wake generator

1.0   Introduction

Weight and efficiency are important factors in aircraft design and performance. The performance of an aircraft is linked to its weight and engine efficiency. Payload capability is increased through weight reductions in the engine and more efficient engines reduce operating costs. The engine weight can be reduced by decreasing the axial gap between blade rows in the compressor. The smaller axial spacing makes for a more compact engine, thereby making the aircraft configuration layout easier. The effects of compressor blade row spacing on the stage efficiency has been studied, but yield mixed results. This study investigates the affects on span-wise efficiency of reducing the axial spacing between a stator and rotor blade row in a transonic compressor, with emphasis places on the tip region of the rotor blade.

1.1   Overview of Turbomachinery

Turbine engines provide the main source of thrust for most military and civilian aircraft. Thrust in turbine engines is achieved in two ways: accelerating the air flow through the engine and pressure differentials between the inlet and outlet. In both methods, the engine performs work on the air flow. The primary components of a typical turbine engine are an inlet, compressor, combustor, turbine, and exit nozzle. A diagram of a turbine engine is provided in Figure 1.1.1.

The addition of work to the air flow is accomplished by two components: the compressor and combustor. The compressor's purpose is to increase the pressure of the fluid, thereby increasing the enthalpy of the flow using a succession of stators and rotor blade rows. The combustor injects fuel into the air flow and ignites the mixture to release chemical energy stored in the fuel, causing an increase in temperature of the air flow (Mattingly, 1996). The present study focuses on the compressor component, specifically an axial flow compressor of a transonic turbine engine.

1.2   Compressor Design

The compressor is designed to increase the pressure of the incoming air in order to increase the energy of the flow and provide for a more efficient combustion process. This study is performed for an axial compressor. In an axial compressor the air flows in the axial direction through a series of rotor blades, which rotate, and stator vanes, which are stationary. The advantages of the axial compressor are a smaller frontal area and a more compact process than other forms of compressors (Mattingly, 1996). The components of an axial compressor are shown in Figure 1.2.1. The first picture in Figure 1.2 is a series of rotor blades, followed by rows of stator vanes. The final picture in the figure is the combination of rotor blades and stator vanes.

High performance compressors are being designed with the goal of reducing weight and length without sacrificing performance (Gorrell et al., 2002a). This investigation studies the blade interaction effects between a single row of stator vanes and a row of rotor blades as the axial distance is reduced. The closer the blade rows can be spaced, the

more compact the engine can be designed. Smaller engines equate to less weight and are desirable in aircraft design. The trade-off for closer spaced rows is an increase in the unsteady aerodynamic interactions between rows. The unsteady interactions include convective wakes, secondary flows, pressure waves, tip-clearance vortices and shocks. Understanding how the blade rows interact at various axial gaps is an important step in determining the beneficial and detrimental effects of reducing the axial length.

1.3   Importance of Blade Row Interactions and Efficiency

Previous studies have mixed results on the effects closer blade row spacings. If the blade row gap can be decreased, while maintaining or improving the efficiency of current compressors, then the total length of the engine can be reduced. The efficiency of an axial turbine engines is of great interest for many reasons. Better efficiencies mean lower fuel consumption, which in turn means increased the range per a fueling or increased payload capabilities. For private industry, reducing the fuel consumption means reducing the operating costs and greater profits. In military aircraft, increased efficiency allows for greater payload capabilities or increased range. How the blade rows interact must be understood in order to benefit from reduced axial spacing of blade rows.

The interaction between blade rows is necessary for fluid-dynamic compression (Fleeter, 2001). However, compressor performance, operability, and life are affected by these unsteady interactions. The aerodynamic loading of the blades is increased and high-cycle fatigue occurs, both are disadvantages commonly encountered in turbomachinery (Falk,

2003). Understanding the unsteady aerodynamic interactions between blade rows will aide in the design of more efficient turbine engines.

1.4 Factors that affect Efficiency

The present investigation focuses on the influence of unsteady aerodynamic effects on efficiency. Therefore, understanding the flow characteristics used to calculate efficiency is important. Compressor efficiency is calculated using the equation:

$$\eta_C = \frac{\pi_C^{(\gamma-1)/\gamma} - 1}{\tau_C - 1}$$

where the temperature and pressure values used in the temperature ratio and pressure ratio are taken downstream of the compressor stage. From the above equation one can see that increases in the pressure ratio increase efficiency, while increases in the temperature ratio cause a decrease in efficiency. Unsteady aerodynamic interactions that affect the pressure and/or temperature are of interest since those interactions influence the efficiency of the compressor. Additionally, following changes in energy, or entropy, will identify factors that cause a decrease in efficiency.

1.5 Outline of the Thesis

Chapter Two provides a review of past studies that contain highlights of developments in understanding tip clearance flows and the influence of axial gaps on compressor stage performance. Additionally, a summary of the research to date is provided, as is a description of the objectives of the present investigation.

Details of the Stage Matching Investigation rig, used in obtaining experimental data, and an overview of the MSU-TURBO package, used in simulating the SMI rig setup, are explained in Chapter Three. Descriptions of the grid generation software and grid characteristics are also explained in Chapter Three. A brief overview of the post processing and interpretation of the MSU-TURBO output data is covered as well.

Chapter Four presents the results and discusses the findings of the current study. A detailed analysis of the efficiencies versus percent span for both cases is given to better understand the flow characteristics responsible for the efficiency phenomena being studied. Tecplot contour plots are used to give a visual representation of the flow through the rotor passage. A summary of this research and the conclusions from the numerical investigation are presented in Chapter Five.

2.0   Previous Investigations and Studies

This chapter provides a review of previous studies performed in the areas of tip clearance flow, IGV-rotor axial spacing effects, and unsteady blade-row interactions. The intent is to show the importance of tip flow, axial spacing, and unsteady phenomena on the efficiency of the compressor stage and the need for further research in this field.

2.1   Literature Review

Attempts to gain an understanding of the unsteady aerodynamic phenomena in turbine engines have been performed in the past. One of the first studies was carried out by Mikolajczak. Mikolajczak (1976) investigated the effects on compressor performance of changing axial spacing. He noticed an increase in peak efficiency with a close spacing. However, the improved performance could not be explained and further studies into unsteady phenomena in turbomachinery were recommended.

Another investigation completed by Hetherington and Moritz (1977) observed various types of unsteady phenomena in turbomachinery. They found tip clearance leakage flow to be of particular interest because of the high pressure gradient and its ability to influence the boundary layer conditions on the outer casing. Hetherington and Moritz stated that the bulk of all turbulence generated within the compressor was a result of the airfoil wakes, which are intense. Due to wake mixing losses, they suggest that blades rows should be spaced far enough apart to allow wake mixing to sufficiently occur

between blade rows. Their conclusion was that "re-examination of the size of axial gaps may well repay attention for design point efficiency."

Adamczyk et al. (1996) examined unsteady flows and their effects on wake rectification and rotor performance. The research explored the differences between a rotor blade row operating in isolation and a blade row operating downstream of a stator row. The conclusion was a major difference exists between the isolated rotor and the on operating downstream of a stator row. This finding shows the presence of blade-row interactions. Their numerical simulations showed the stator wake mixing within the rotor passage. Radial and tangential momentums of fluid particles were studied and the results presented. The simulation showed the stator wake tendency to drift toward the pressure side of the downstream rotor. This observation agrees with a studies performed by Kerrebrock and Mikolajczak (1970).

Investigation into the modeling of core compressor tip leakage was performed by Glanville (2001). This study tested two turbulence models and different methods for generating a rotor tip grid. The conclusion was a generalized H-mesh used to model the rotor geometry with a square tip resulted in better loss production predictions than the pinched tip method. The Baldwin-Lomax and Spalart-Allmaras turbulence models were compared. Both models over predicted the amount of loss production and no significant advantages were found in using the Spalart-Allmaras model instead of the simpler Baldwin-Lomax model.

A study performed by Chriss et al. (1999) concluded for axial spacing of 50% of the upstream blade chord or more, wake mixing could fully explain the losses in performance. For spacings less than 50% upstream blade chord, the suggested flow loss mechanisms are shock/wake interactions, increased blockage from secondary flows, and three-dimensional effects not accounted for in the experiment. The research was not conclusive on whether loss sources were present at spacings less than 50% chord and was not able to identify the origin or magnitude of any losses for this spacing range.

Gorrell et al. (2002a) ran experimental tests to investigate the effects of blade-row spacing on the performance of a transonic compressor. The researchers studied changes in performance by varying the axial spacing and solidity of the wake generator row. They concluded that the performance was significantly influenced by the position of the upstream stator relative to the downstream rotor. Measurements showed the mass flow rate, pressure ratio, and efficiency all decreased with a reduced axial gap between the stator vane row and rotor blade row. This observation was noted to be contrary to the concept of wake recovery, which states smaller axial gaps reduce mixing losses and allow the wake to be reversibly flatted thereby reducing the entropy production from viscous dissipation. Increased solidity of the upstream wake generator blade-row also decreased the pressure ratio and efficiency of the compressor stage.

Further studies by Gorrell et al. (2002b) focused on the influences of the rotor bow shock on the compressor stage performance at various axial spacings. They suggest the MSU-TURBO code provides a conservative estimate of the blade-row interactions loss because

the simulated pressure wave was weaker than the pressure wave measured experimentally using the Stage Matching Investigation Rig (SMI). The results from the study by Gorrell et al. concluded the loss production is dependent on the strength of the rotor bow shock when it impacts the trailing edge of the upstream wake generator.

A study by Sirakov and Tan (2002) investigated the interactions between the stator wake and the rotor tip clearance flow using unsteady three-dimensional Reynolds-averaged Navier-Stokes simulations. The authors focused on the rotor tip region and considered a full stator-rotor calculation to be unnecessary. The rotor performance was found to benefit from interactions with the upstream stator wake. The improved performance was linked to a phenomenon called double leakage, usually occurring in highly loaded blade-rows. The authors suggest designs with decreased axial gaps between blade rows can benefit from greater upstream unsteadiness.

Zachcial and Nürnberger (2003) performed a detailed numerical study of the effects of axial spacing between blade-rows in a compressor stage at both subsonic and transonic conditions. The subsonic case displayed a trend opposite to those observed in experimental investigations. For subsonic conditions, an increase in compressor performance corresponded with an increase in the axial gap. At transonic operating conditions an increase in performance was observed when the blade-rows were closer together, which is in opposition to the findings of Gorrell et al. (2002a). A vortex pattern near the suction side of the rotor blade was detected at both operating condition and noticed to rotate clockwise. For the transonic operating point, the vortex was noticed to

have the beneficial result of reducing the boundary layer separation flow for the suction side of the rotor. The mechanism responsible for this effect is the reduction of the pre-shock Mach number, which precipitates a decrease of the losses from the shock in the rotor passage. This mechanism is concluded to be main reason for the trend in stage efficiency.

2.2   Summary of Past Investigations

Several investigations have been performed studying the effects of tip clearance flow and axial spacing between blade-rows on compressor performance. Mikolajczak (1976), Sirakov and Tan (2002), and Zachcial and Nürnberger (2003) found closer spacings to be beneficial, while Hetherington and Moritz (1977) and Gorrell et al. (2002a) observed a decrease in efficiency at closer spacings. Only in recent years have studies of blade-row interactions been examined in transonic flow conditions. Early studies focused on subsonic flows through turbine engines. The investigation performed by Zachcial and Nürnberger (2003) compared the performances of subsonic and transonic operating conditions. Their results show that subsonic flows have opposite trends than the transonic flows. However, the findings of Zachcial and Nürnberger are contrary to the results of the investigation by Gorrell et al. No agreement on the influence of axial spacing between blade-rows for transonic simulations and experiments has been reached.

2.3   Areas for Further Research

Further research into the physical mechanisms and unsteady aerodynamic flow associated with close blade-row spacings is needed to better understand benefits and disadvantages.

A sensitivity study of the influence of axial spacing on performance may clarify the relationship between the magnitude variations of the unsteady aerodynamics and gap size. The effects of blade interactions at various spans warrant additional investigation. If the beneficial effects at certain spans are identified, then the blade geometry can be changed to remove detrimental effects for the remainder of the blade while keeping advantageous characteristics.

2.4   Objectives of the Present Investigation

The current investigation is a study of an interesting phenomena discovered in the research performed by Gorrell et al. in 2002. Analysis of their experimental data revealed a local increase in efficiency near 90% span at reduced spacing between blade rows. This situation is contrary to the rest of the spans. The current investigation examines the effects of axial spacing between blade rows on the span-wise efficiency of an axial compressor stage operating at transonic flow conditions in an attempt to identify the physical mechanism responsible. Using three-dimensional, time-accurate, Reynolds-averaged Navier-Stokes simulations, the influence the axial gap has on the fluid flow through the compressor stage is studied. The simulations are performed using a parallel, multi-block flow-solver called MSU-TURBO. The objectives are:

1. Develop and implement a computer program to read the output data files from the MSU-TURBO flow-solver and calculate the necessary flow variables for further analysis.

2. Assess the ability of the MSU-TURBO simulations to capture the local increase in the near-casing efficiency observed in experimental SMI rig tests.

11

3. Generate new grid input files, with increased tip clearance nodes that better capture tip clearance flow, to be used in further analysis of transonic compressor stage efficiency by the Air Force Research Laboratory.

4. Investigate the physical mechanisms responsible for span-wise differences in stage efficiency between the Close and Far blade row axial spacings.

3.0   Computational Methodology

This chapter contains detailed information on the setup and methodology used in the current computational investigation. Information is provided on the Stage Matching Investigation (SMI) rig used in obtaining the experimental data for which the MSU-TURBO flowfield solution is compared. The 3D computation fluid dynamics code MSU-TURBO is described, along with a discussion of input parameters, grid generation, and boundary conditions.

3.1   Stage Matching Investigation Rig

The Stage Matching Investigation (SMI) Rig is an experimental compressor rig operated by the U. S. Air Force in their Compressor Aero Research Lab (CARL) at Wright-Patterson Air Force Base, OH. The SMI rig is a compressor with three blade rows: a wake generator, rotor, and stators. The compressor is designed for high-speed and high-loading conditions with the ability to vary the wake generator-to-rotor axial spacing and the wake generator blade count (Gorrell et al, 2001). Figure 3.1.1 shows a cross sectional view of the SMI rig. The design of the wake generators (WGs) is to simulate typical wakes produced in modern, highly loaded, lo-aspect-ratio, front-stage compressor stators. In order to simplify the experiment, the wake generators use an uncambered, symmetric airfoil that produces a large base drag, but does not cause swirl in the flow. Additionally, the airfoil used for the wake generators has a small leading edge radius and a relatively blunt trailing edge radius (Copenhaver et al, 2001). The wakes produced by the WGs are

turbulent and do not decay as rapidly as wakes produced by high-aspect-ratio stages with lower loading (Gorrell et al, 2002a). Isolation and simplification of the wake characteristics during the experiment was achieved through the design of the WGs. The WGs design attempted to reproduce two-dimensional wakes similar to wakes reported by Creason and Bagdadi (1988). The stator and rotor-blade rows of the SMI rig were designed by Law and Wennerstrom (1989) at the CARL facility and were fabricated by Pratt & Whitney (Chriss et al., 1999). Design parameters can be found in Table 3.1.1.

Typical axial spacing for current operational fans and compressors is represented by the Far spacing configuration. While the WG blade count could be varied, for this study the WG blade count was set at 24. The chord is varied from hub to tip in order to maintain constant solidity. This variation is done to hold span-wise loss and wake width constant (Gorrell et al., 2002a).

3.2   MSU-TURBO Overview

MSU-TURBO is a three-dimensional time-accurate flow solver specifically designed for analysis of unsteady turbomachinery phenomena. MSU-TURBO is a computational fluid dynamics package that solves the Reynolds averaged Navier-Stokes equations in a rotating reference frame using an implicit finite-volume solver. The turbulence model employed by MSU-TURBO was developed by the Institute for Computational Mechanics in Propulsion (ICOMP) at NASA Glenn Research Center. The turbulence model uses low Reynolds number k-ε eddy viscosity models along with wall functions (Zhu et al., 1997).

The solution is partitioned into sub-domains for parallel processing. Single-program multiple-data parallelization allows each flow sub-domain to be solved separately on a dedicated processor. Flow variables at sub-domain interfaces are updated using Block-Jacobi updating and symmetric Gauss-Seidel iterations (Chen et al., 2001).

Due to the relative motion between the wake generators (stationary) and the rotor blade (rotating) grids, a dynamic sliding-mesh model is used to separate the two grids. Phantom cells are used within the dynamic sliding-mesh model to interpolate the fluid values for cells at the interface boundary between the two blade rows. A buffer ring is created by the phantom cells comprised of a circumferential array of data relating each neighboring blade row (Chen et al., 2001). Once extracted, the data in the buffer ring is sent to the processor governing the solutions in the neighboring sub-domains, which are on the other side of the sliding-mesh interface. The sub-domain boundary conditions are then updated by using interpolated values from the sub-domain and the transferred data array (Darbe, 2004).

The number of flow passages required to capture the flow characteristics of the compressor is dependant on the ratio of vane-to-rotor blades. Compressors with an equal number of vane blades and rotor blades can be modeled with only one flow passage for each vane/rotor row. However, the SMI rig from which the computational model was created has a ratio of vanes-to-rotor blades less than one. The compressor has 24 wake generators blades and 33 rotor blades. Thus, the solution requires more than one flow

passage for each vane/rotor row. For vane/rotor ratios greater than one, the compressor can be either modeled as a full annulus or broken into symmetric sections. With a 24/33 vane/blade count, the annulus can be divided into 3 sections each containing 8 vanes and 11 rotor blades. The 8/11 vane/blade section can be solved and duplicated to generator a solution for the full annulus. The computational time required to solve a 8/11 vane/blade section is higher than a one-to-one ratio, but is drastically less than modeling the full annulus.

Another method of handling unequal vane/rotor counts is to apply a phase lag condition to the boundary. MSU-TURBO supports such a method, thus allowing the model to be reduced down to one flow passage per vane/blade row. This method of modeling the compressor greatly reduces the computational time required for convergence. The phase-lag boundary conditions cause different inlet/outlet areas along the sliding-mesh interface for each vane/blade row. The time-varying flow-history at the interface is stored by MSU-TURBO and extracted to create a buffer ring for interpolating between adjacent sub-domains. The amount of flow-history stored by MSU-TURBO during execution is an input variable defined by the user (Chen et al., 2001). While the computational time is decreased using the phase-lagged boundary conditions, the blade-row interactions are approximated at neighboring blade-passing frequencies and their harmonics. This approximation causes a loss of flow information for blade-row interactions not related to blade-passing frequencies (Darbe, 2004).

The inlet and outlet of the compressor were set to standard atmospheric pressure. Wall boundary conditions were applied the hub, casing, and vane/blade surfaces. An open mesh with phase-lagged boundary conditions was used to model the tip clearance between the rotor blade and outer casing.

Previous investigations have successfully used the MSU-TURBO solver to model turbomachinery phenomena. Most relevant to the current study is the work performed by Gorrell et al. (2001) in modeling the SMI rig to investigate the effects of stator-rotor interactions in a transonic compressor. Gorrell et al. produced computational results that agreed with experimental measurements of flow behavior. Other researchers having used the MSU-TURBO software include Van Zante (1997), Barter et al. (1998), and Panovsky (2000). Van Zante (1997) computed time-averaged results from both MSU-TURBO and experimentally. Comparing the results Van Zante found excellent agreement between the computational data and the experimental, but found higher vane-wake dissipation rates in the computational results than in the experimental measurements. Barter et al. (1998) noted accurate first- and second- harmonics frequencies in a comparison of MSU-TURBO and experiment results. Panovskey et al. (2000) concluded that MSU-TURBO simulation results compared agreeably with experimental measurements. These previous studies validate the accuracy of the MSU-TURBO package for the current investigation of time-accurate blade-row interactions.

Detailed input and output information for MSU-TURBO can be found in Appendix C and D, respectively.

3.3 Grid Description

An average passage model developed by Adamczyk is used to model the compressor stage. Using this model, the adjacent blade rows are accounted for through an average passage flow-field representation (Gorrell et al., 2002a). Details of the grid are discussed in the following sections.

3.3.1 Average Passage Grid Software

The Average Passage Grid (APG) software is a mesh-generation algorithm developed to provide suitable grids for APNASA (Beach, 2003), but can also be used to generate grids for MSU-TURBO. The grids used in the current computational study were created with APG. APG creates a single, blade-passage centered grid block using a structured H-type grid. The user defines the compressor geometry in several text file databases, which are used to generate an axisymmetric (axial-radial) profile of the blade rows. The text file databases allow the user to control the grid density, sliding-mesh interface location, elliptical smoothing parameters, tip clearance properties, etc. A user guide and example input files are given in Appendix C. The axisymmetric profile is rotated by the appropriate blade-row pitch to create the final three-dimensional grid (Falk, 2003). All the grids used in the current study employ elliptical smoothing. Elliptically smoothing the grid configuration reduces the number of skewed grid cells, which improves the accuracy and convergence of the computations (Darbe, 2004).

3.3.2 Grid Characteristics

The current study employs three different grids: two wake generator grids and one rotor grid. The difference between the wake generator grids is the distance from the trailing

edge to the outlet plane, which creates the two cases: Close and Far. The same rotor grid was used for both the Close and Far spacing cases. The compressor inlet, rotor exit plane, and the outer radius are kept constant between the Close and Far cases. The indices i, j, k are used to represent the grid points in the axial, radial and circumferential directions, respectively. Further information on the grids is tabulated in Table 3.3.1.

3.4   Computation Fluid Dynamics Setup

The numerical simulations were run with a rotor speed of 13,509 RPM and 270 time steps per blade-passing period. Dependent variables were iteratively calculated during each time step. When variations in the mass-flow rate and vane surface-pressure fell below 0.1% the solution was considered to be converged.

3.4.1   Computational Reference Values

MSU-TURBO operates using non-dimensionalized variables. The reference values used for both the MSU-TURBO simulation and the post-simulation analysis are listed in Table 3.4.1.

3.4.2   Simulation Boundary Conditions

Isentropic subsonic inlet flow was used for the inlet boundary condition and was accomplished using radial profiles of total pressure; all other variables were held constant with radius. Hub and casing boundary layer behavior was simulated by specifying total pressure values at a range of span-wise locations. The reference values and boundary

conditions are entered into MSU-TURBO by way of input text files created by the user. Examples of the text files can be found in Appendix C.

3.5 Interpretation of Data

After the numerical simulations are complete, the data must be processed into a usable format. The output files from the MSU-TURBO solver contain a limited number of variables. From the output variables, all other flow variables can be calculated. The flow-field variables are then written to a Tecplot formatted file where graphical plots of the rotor passage can be analyzed further.

4.0 Results and Discussion

This chapter presents the numerical results from analysis of the MSU-TURBO simulations and discusses the span-wise differences between the Close and Far cases.

4.1   Analysis of MSU-TURBO Output Information

Data from the MSU-TURBO output files provided by the CARL group at WPAFB was extracted using several FORTRAN codes specifically developed for this task.   The format of the flow-field solution files is given in Appendix D. Two time-averaged, 3D flow-field solution files were generated from the 40 time-step files for the Close case and 60 time-step files for the Far case.   The 40 and 60 files for the Close and Far cases, respectively, represent two blade passes. The time-averaged files are used to generate the time-averaged flow-field variables of interest, such as temperature, Mach number, etc. The flow-field information was then written to a new file in Tecplot format. The Tecplot format is described in Appendix E. Using the Tecplot program and flow solution files, contours of any variable in the rotor passage can be displayed. The codes developed for the extraction of flow-field information were compared against hand calculations of the data and found to be match. Therefore, the code is performing the proper calculations operations and storing the data successfully.

4.2   Assessment of Axial Spacing on Compressor Stage Efficiency

The inlet total temperature and total pressure were obtained by finding the mass-averaged values for the inlet plane. The span-wise efficiency was found using the inlet total pressure and total temperature and the average temperature and average pressure values at several spans one chord downstream of the rotor blade. This task was accomplished using a computer code developed during the course of this investigation. The graph of the efficiency one chord downstream versus percent span of the rotor blade shows a large difference between the Close and Far spacing cases around the mid-span region. The plot of efficiency versus percent span is shown in Figure 4.2.1. The trends between the hub, 0% span, and 5% span are the same for both cases. This situation occurs because the boundary layer flow at the hub is approximately the same for both axial locations. Around 8% span, the Close case efficiency starts to decrease, while the Far case efficiency continues to increase with span until 20%. However, between 30% and 70% span for the Close spacing case shows the existence of additional loss mechanisms over those present in the Far case. After 70% span, the trends between the two cases become similar again.

The graph of compressor stage efficiency generated from the numerical simulations does not show the local increase in efficiency observed in the experimental tests near the casing. The initial hypothesis was the tip leakage flow in the Close case increased the efficiency in the near casing region of the rotor blade. An analysis of the tip clearance flow was performed to assess whether the flow was accurately modeled. The assessment of the tip clearance modeling is given in the next section.

Further analysis was needed around 8% span to determine the difference between the Close and Far cases, as well as investigating the large variation between the cases in the mid-span region. In order to study these areas more thoroughly, plots of temperature ratio and pressure ratio versus percent span were generated. The pressure and temperature ratios versus percent span graphs are shown in Figure 4.2.2 and Figure 4.2.3, respectively. The temperature ratio versus percent span graph displays less fluctuations between the Close and Far spacings than does the pressure ratio versus percent span plot. In general, the Close case has a lower temperature ratio than the Far case, except for the mid-span region. The two cases have similar trends from the hub to 20% span, but the magnitude of the temperature ratio for the Close case is lower than the Far case. This situation results in the Close case having a slightly higher efficiency at the lower spans. In the mid-span region, the Close case has a higher temperature ratio than the Far case, which causes the low efficiency. This region is the major difference between the two cases. Similarities in the trends for the cases resumes around 73% span. The graphs of the temperature ratios would be the same with the Close case exhibiting a lower ratio if not for the mid-span values.

The pressure ratio versus percent span graph shows a large difference between the Close and Far cases. The Close case pressure ratio varies greatly with span relative to the Far case fluctuations. The trend between 0 – 10% span for both cases is similar with the Close pressure ratio slightly lower than the Far. However, the Close case ratio continues to decrease after 10% span, while the Far case starts to stabilize around 1.9. In order to

isolate the reason for the fluctuations in the Close case, several radial slices were extracted from the 3D solution at spans that would illustrate the differences between the axial spacings. Results from the analysis of these radial slices are covered in section 4.4.

4.3   Assessment of Tip Clearance Adequacy

A study by Van Zante et al. provides guidelines for achieving accurate numerical modeling of tip clearance flows in transonic compressor rotors. To determine the number of nodes necessary to accurately calculate the tip clearance flow the velocity difference value needs to be found. A normalized velocity difference between the casing and leakage jet is defined by the parameter:

$$VD = \frac{\left(V_{jet} - V_{wall}\cos\gamma\right)}{V_{wall}}$$

where the V_{wall} is the blade tip speed, V_{jet} is the leakage flow velocity, and γ is the angle between V_{wall} and V_{jet}. For the cases run by Van Zante et al., a velocity difference value of $VD = 0.2$ or higher indicates the wall-shear layer is of sufficient strength to influence the primary tip clearance flow. The velocity difference for the Close and Far case was calculated. The wall-bounded shear layer was found to be large enough to require additional nodes in the tip clearance gap. A recommendation of increasing the tip clearance nodes from 8 to 16 was made for future simulations.

4.4   Radial Analysis of Rotor Passage Flow

Radial slices of the three-dimensional flow-field solution were taken for both the Close and Far cases in order to better understand what occurs in the rotor passage. The contour

plots of entropy are shown in Figure 4.4.1 through Figure 4.4.23 at the span values of interest. Each figure shows the slice of the Close axial spacing with the corresponding cut from the Far case. Examining the flow-field differences between the Close and Far cases reveals the reasons for the dissimilarity in the graphs of temperature ratio, pressure ratio, and efficiency versus percent span. The WG wake can easily be seen in the rotor passage in the mid-span region for the Close case. The wake from the upstream WG is allowed to mix with the higher velocity passage flow prior to the rotor passage in the Far case. A large amount of rotation is present in the wakes because of the difference in velocity between the boundary layer separation and the mainstream flow. Viscous shear forces between the two flows cause them to mix, resulting in a loss of total pressure. The efficiency of the stage is decreased with increases in total pressure losses. The wake swirl generates a greater radial motion, causing the wake to drift towards the pressure side of the adjacent rotor blade. If the wake interacts with the boundary layer on the rotor, the flow can transition from laminar to turbulent flow earlier. The turbulent flow encourages additional mixing, and therefore additional total pressure losses. The Close case radial slices show the upstream WG wake near the boundary layer on the pressure side of the rotor blade, and at upper spans, the wake actually merges with the boundary layer separation. This interaction increases the amount of entropy production which in turn reduces the efficiency for the given span. No indication of the WG wake is visible in the rotor passage for the Far spacing case. The interaction between the upstream wake and the boundary layer on the rotor appears to be the main source of difference between the Close and Far cases.

4.5 Axial Analysis of Rotor Passage Flow

In order to gain a better understanding of the rotor passage flow, axial slices of the flow-field solution were taken. Flow in the radial slices was cross-referenced with the axial cuts to determine the source(s) of the efficiency losses. While the radial slices provide flow information in the axial and transverse plane at certain spans, investigation of the tip clearance flow requires examination of the axial slices, which provide flow-field information in the radial and transverse plane.

Figures 4.5.1 through 4.5.9 show the axial cuts from 25% chord to about 31% chord downstream of the trailing edge of the rotor from hub to casing. These figures display the tip leakage flow for the Close (left) and the Far (right) cases. At 25% chord, the WG wakes are visible as diagonal bands of light yellow in the Close case, while no wakes are apparent in the Far case. The boundary layer at the outer casing is similar for both spacings, but the thickness is deeper in the Close case. The tip vortex starts to become visible in the Close case around 31% chord. However, in the Far case, the tip vortex does not start to appear until about 65% chord. Both tip vortices spiral hubward causing great mixing in the flow. With the Close case tip vortex emerging earlier than the Far case, the vortex is able to drift farther toward the hub. The tip vortex moving to lower spans contributes to the efficiency losses in the mid-span region. The Far case tip vortex develops farther along the chord of the rotor and is not as strong as the Close case. Therefore, the influence of the tip flow is less for the Far case and as a result the total pressure losses are also less.

4.6 Comparison of Results with Past Studies

The drift of the WG wake toward the pressure side of the rotor blade agrees with the findings of Hetherington and Moritz (1977). They found the tip leakage flows to have a large influence on the outer casing boundary layer. Hetherington and Moritz recommended spacing of the blade rows far enough apart to allow for the majority of the mixing to be accomplished between the rows. The data from the present investigation concurs with the assessment of Hetherington and Moritz that the axial distance between the blade rows should allow for mixing to occur prior to entering the rotor passage. Additionally, the tip flow noticed in the present research shows a significant impact on the casing boundary layer, which supports the findings of Hetherington and Moritz.

The efficiency decease at reduced spacings agrees with the research performed by Gorrell et al. (2002), but does not show the same local increase in efficiency in the near casing region. However, the decrease in compressor efficiency found is contrary to the findings of Zachcial and Nürnberger (2003). They found an increase in compressor efficiency with reduced axial spacings. The difference in the trends may be explained by the method in which the flow-fields were modeled. Both the present study and the one done by Gorell et al. used three-dimensional flow-fields, while the simulations of Zachcial and Nürnberger focused on a two-dimensional representation near the casing.

Studies of the effects of axial distance on the compressor efficiency have produced mixed results. The influence of the axial spacing and the tip leakage flow on the compressor

efficiency is of particular interest and warrants further study. Specifically, research on the near casing region of the rotor blade would be beneficial.

5.0 Conclusions

This study numerically examined the span-wise efficiency of a transonic compressor stage representative of a modern jet engine. Two simulations of a compressor stage with different axial spacing between blade-rows were studied to determine the influence on the fluid flow. The two spacing are denoted as Close and Far. The time-accurate Reynolds-averaged Navier-Stokes computational algorithm MSU-TURBO with a CMOTT turbulence model was used for both cases. All solutions are three-dimensional and model WG-rotor relative motion through a sliding-mash interface and phase-lagged boundary conditions.

At reduced spacings the compressor stage is less efficiency, with the largest difference occurring in the mid-span region. One reason for this trend is the wake from the upstream wake generator does not completely mix with the main passage flow prior to entering the rotor passage with decreased axial gaps. The wake entering the rotor passage influences the boundary layer on the rotor blade causing the flow to transition to turbulent flow sooner than if the wake was allowed to mix sufficiently with the main stream. The turbulent flow results in greater entropy production and increased total pressure losses, ultimately causing a loss in efficiency. The reduced spacing may cause an increase in strength of the blade-row unsteady interactions, which would require a greater distance to dissipate. This situation further complicates the flow at reduced spacings.

The other major unsteady factor identified that influences the compressor efficiency is the tip clearance flow. Through slices taken at constant axial distance, the tip clearance flow was found to drift toward the hub. In the Far case, the tip vortex did not reach spans below 80%. However, for the Close case, the tip vortex reached to around 40% span. Examining the flow one rotor chord downstream revealed the region between 40% and 60% span to be the main difference between the two axial spacings. Additionally, the rotor tip leakage at the reduced spacing occurs around 30% chord, while the Far casing leakage flow does not appear until 50% chord. The consequence of the early appearance of the tip vortex in the Close case is the greater axial distance that the vortex has to drift to lower spans. The greater strength of the Close spacing leakage flow over the Far case may be another reason the vortex is able to influence the mid-span region.

The conclusions reached in this analysis are: the upstream wakes interact with the rotor boundary layer and the tip flow is a major factor at reduced spacings. The purpose of this study was to identify the reasons for efficiency losses, therefore further investigations into the correlation between axial spacing and efficiency loss are needed.

6.0 References

Adamczyk, J.J., Celestina, M. L., Chen, J. P., 1996, "Wake-Induced Unsteady Flow: Their Impact on Rotor Performance and Wake Rectification," ASME Journal of Turbomachinery, Vol. 118 January 1996, pp. 88 - 95

Chen, J. P., and Briley, W. R., 2001, "A Parallel Flow Solver for Unsteady Multiple Blade Row Turbomachinery Simulations," ASME Paper 2001-GT-0348, ASME Turbo Expo 2001, New Orleans, LA, June 2001

Chriss, R. M., Copenhaver, W. W., Gorrell, S. E., 1999, "The Effects of Blade-Row Spacing on the Flow Capacity of a Transonic Rotor," ASME Paper No. 99-GT-209

Copenhaver, W. W., Estevadeordal, J., Gogineni, S., Gorrell, S., Goss, L., 2001, "DPIV study of near-stall wake-rotor interactions in a transonic compressor", 4th International Symposium on Particle Image Velocimetry, Göttingen, Germany, September, 2001

Darbe, R. P., 2004 "Influence of Trailing-Edge Geometry on IGV Forced Response in a Transonic Compressor", Oklahoma State University, July 2004

Falk, E. A., 2003, "Influence of Unsteady Blade-Row Interactions on Tip-Efficiency in a Transonic Compressor", Air Force Summer Faculty Fellowship Program Final Report, Summer 2003

Fleeter, S., 2001, Guest Lecture, Proceedings of the 6th National Turbine Engine High Cycle Fatigue Conference, Jacksonville, FL.

Gastineau, Z. D., 2002, "Turbine Engine Performance Improvements – A Proactive Approach," ASME Journal of Turbomachinery, Vol. 124 April 2002, pp. 223-226

Glanville, J. P., 2001, "Investigation into Core Compressor Tip Leakage Modeling Techniques using a 3D Viscous Solver," AMSE Paper No. 2001-GT-0336, AMSE Turbo Expo 2001, New Orleans, Louisianna

Gorrell, S. E., Okiishi, T. H., and Copenhaver, W. W., 2002a, "Stator-Rotor Interactions in a Transonic Compressor Part 1 – Effect of Blade-Row Spacing on Performance," ASME Paper No. GT-2002-30494, AMSE Turbo Expo 2002, Amsterdam, The Netherlands.

Gorrell, S. E., Okiishi, T. H., and Copenhaver, W. W., 2002b, "Stator-Rotor Interactions in a Transonic Compressor Part 2 – Description of a Loss Producing Mechanism," ASME Paper No. GT-2002-30495, AMSE Turbo Expo 2002, Amsterdam, The Netherlands.

Hetherington, R. and Moritz, R. R., 1977, "The Influence of Unsteady Flow Phenomena on the Design and Operation of Aero Engines," Unsteady Flow Phenomena in Turbomachinery, AGARD CP – 177, North Atlantic Treaty Organization

Kerrebrock, J. L. and Mikolajczak, A. A., 1970, "Intra-stator Transport of Rotor Wakes and Its Effect on Compressor Performance," ASME Journal of Engineering for Power, Vol. 92A, pp. 359-368

Mattingly, J. D., 1996, Elements of Gas Turbine Propulsion, New York, McGraw-Hill, Inc.

Mikolajczal, A. A., 1976, "Practical Importance of Unsteady Flow," Unsteady Flow Phenomena in Turbomachinery, AGARD CP – 177, North Atlantic Treaty Organization

Sirakov, B. T. and Tan, C. S., 2002, "Effect of Upstream Unsteady Flow Conditions on Rotor Tip Leakage Flow," ASME Paper No. GT-2002-30358, ASME Turbo Expo 2002, Amsterdam, The Netherlands

Van Zante, D. E., Strazisar, A. J., Wood, J. R., Hathaway, M. D., and Okiishi, T. H., 2000, "Recommendations for Achieving Accurate Numerical Simulation of Tip Clearance Flows in Transonic Compressor Rotors," ASME Journal of Turbomachinery, Vol. 122, October, pp. 733-742

Zachcial, A. and Nürnberger, D., 2003, "A Numerical Study on the Influence of Vane-Blade Spacing on a Compressor Stage at Sub- And Transonic Operating Conditions," ASME Paper No. GT2003-38020, ASME Turbo Expo 2003, Atlanta, Georgia

7.0 Appendices

Appendix A: Tables

Table 3.1.1: SMI Aerodynamic Design Parameters (Gorrell et al., 2001)

SMI Parameter	Blade Row
Number of Airfoils	33
Inlet Hub/Tip Ratio	0.750
Flow/Annulus Area	195.2991 $^{kg-m2}$/s
Flow/Unit Area	85.4531 ^{kg}/$_{s-m2}$
Leading Edge Tip Diameter	0.4825 m
Leading Edge Hub Diameter	0.3620 m
Trailing Edge Tip Diameter	0.4825 m
Trialing Edge Hub Diameter	0.3872 m

Table 3.3.1: Grid Dimensions and Information

Case	Grid Size	Leading Edge	Trailing Edge	Tip
Wake Generator - Close	(i,j,k) = (138,71,61)	i = 31	i = 111	j = 71
Wake Generator – Far	(i,j,k) = (190,71,61)	i = 23	i= 103	j = 71
Rotor	(i,j,k) = (189,71,81)	i = 19	i = 99	j = 63

Table 3.4.1: Reference Values

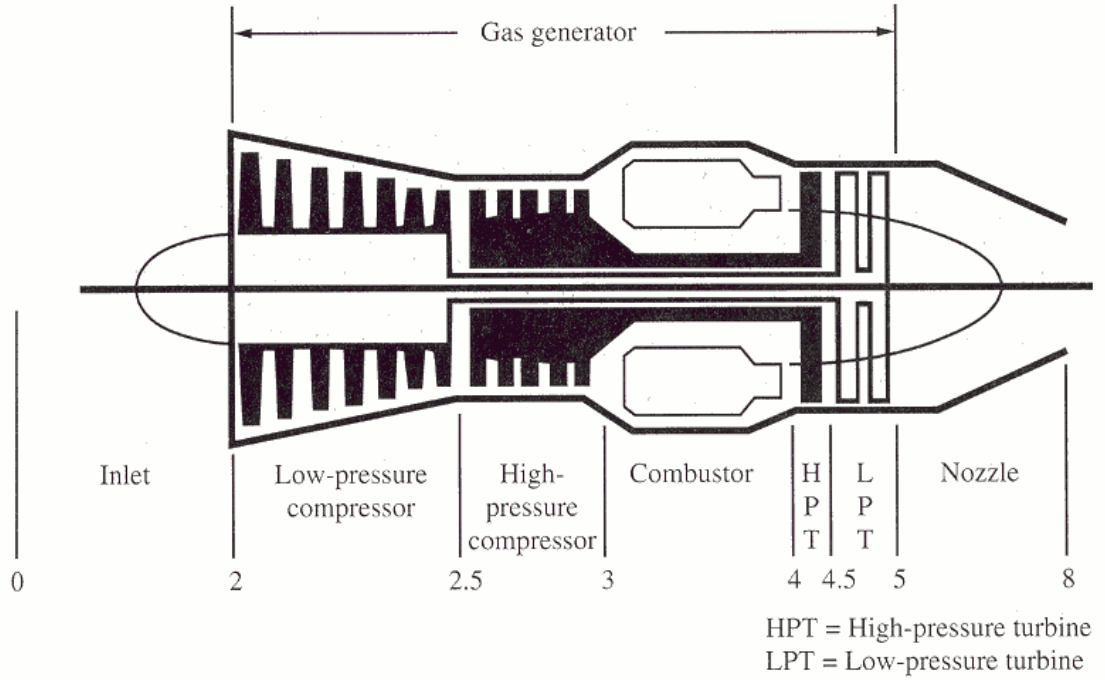| Reference Parameter	Value
Rotor Rotational Speed	1414.65917191 rad/s
Pressure	101325.39296 Pa
Length (Outer Diameter)	0.4826 m
Temperature	288.15 ^{o}K
Velocity	287.596357464 m/s
Gas Constant	287.04377868 N-m/kg-s
Gamma	1.40147

Appendix B: Figures

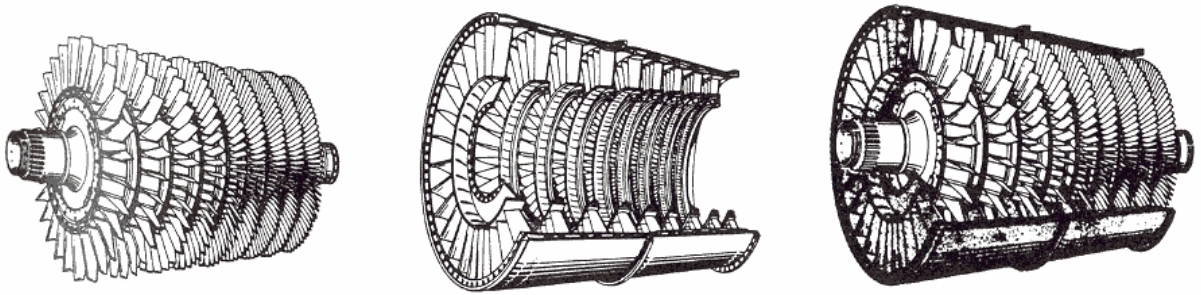**Figure 1.1.1: Diagram of a Turbine Engine (Mattingly, 1996)**

Figure 1.2.1: Example of an Axial Compressor (Mattingly, 1996)

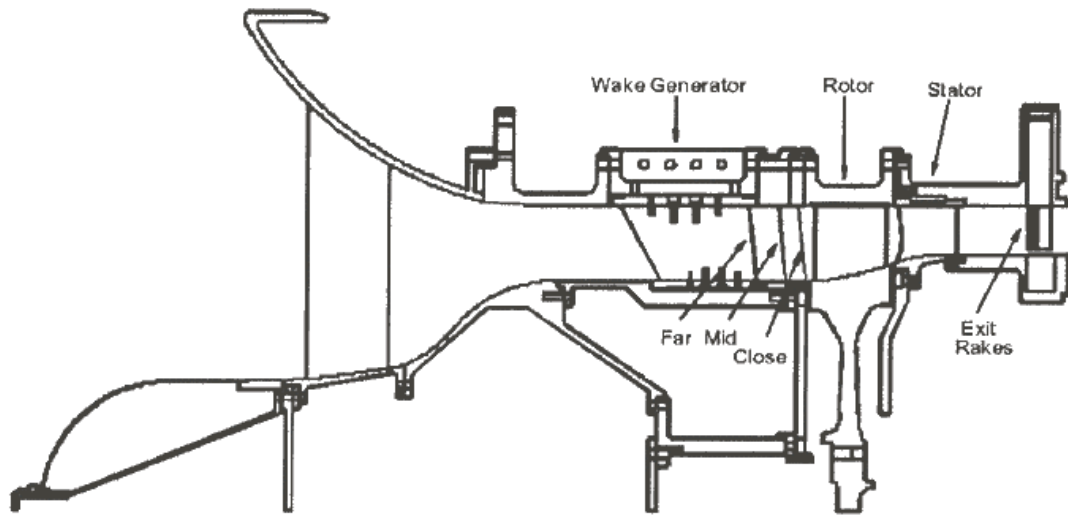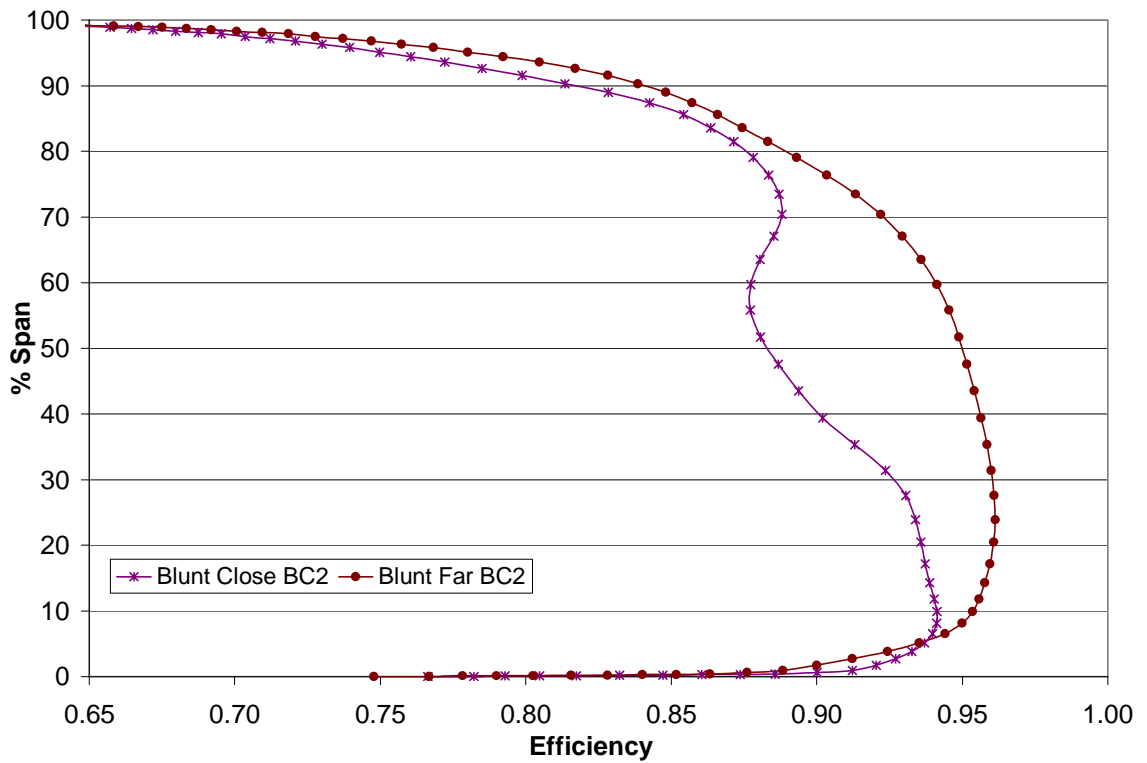**Figure 3.1.1: Cross-Sectional View of the SMI Rig (Gorrell et al., 2001)**

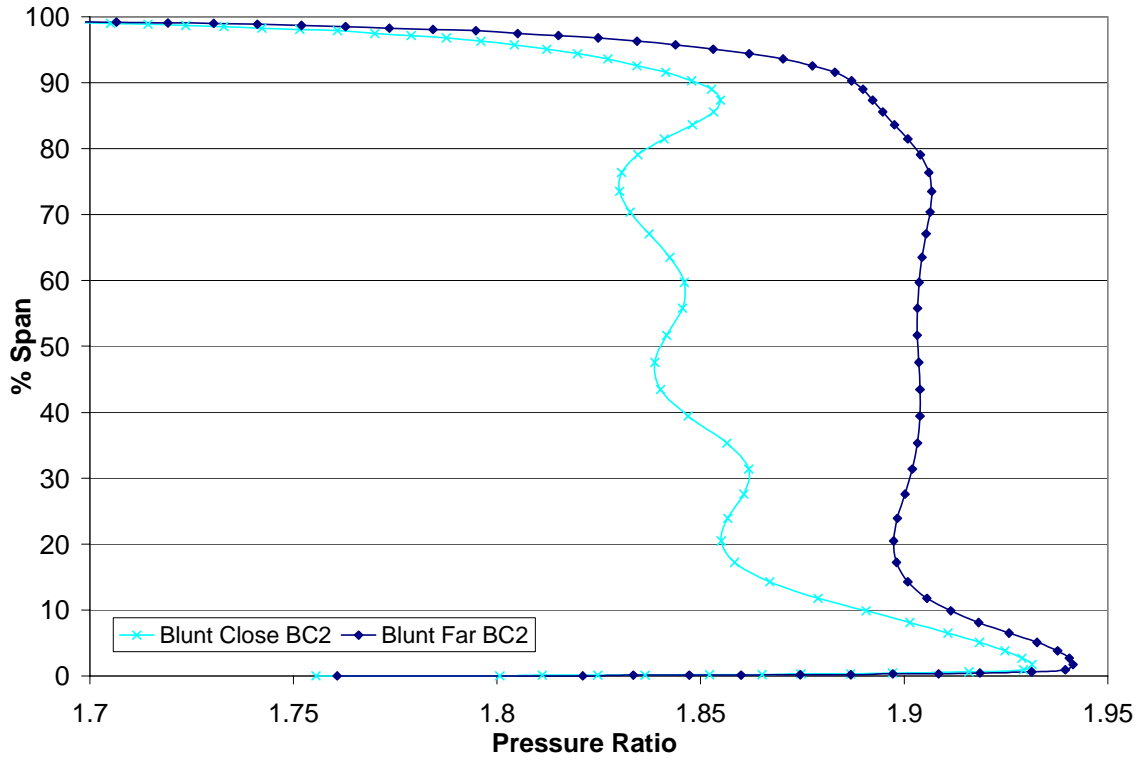**Figure 4.2.1: Efficiency versus Percent Span for Close and Far spacing**

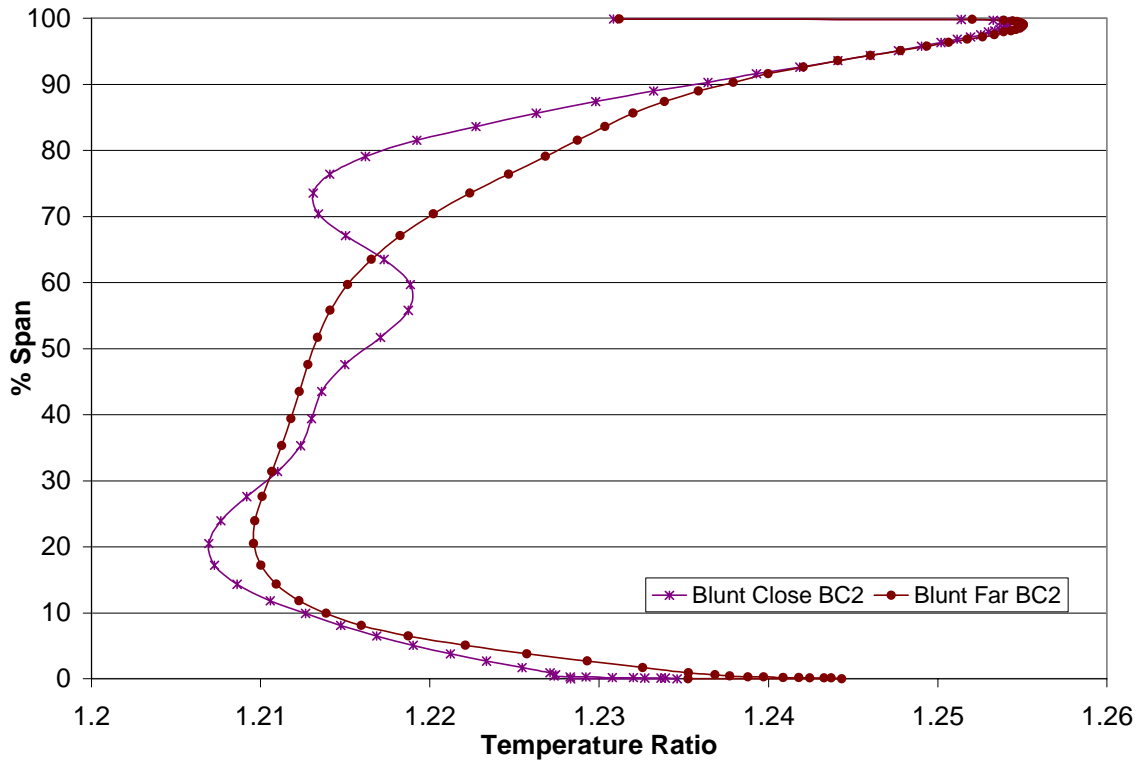**Figure 4.2.2: Pressure Ratio versus Percent Span for Close and Far spacing**

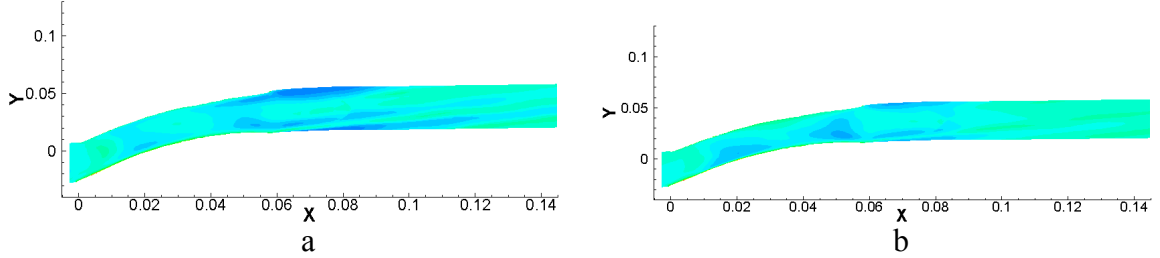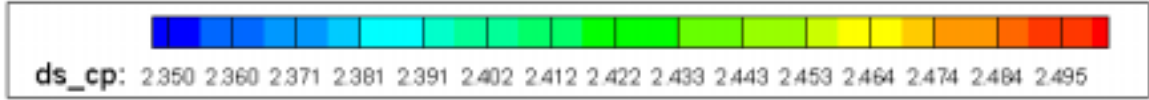**Figure 4.2.3: Temperature Ratio versus Percent Span for Close and Far spacing**

Figure 4.4.1: Entropy Radial Slice at 1.7% Span a.) Close Spacing b.) Far Spacing

Figure 4.4.2: Entropy Radial Slice at 5.1% Span a.) Close Spacing b.) Far Spacing

Figure 4.4.3: Entropy Radial Slice at 9.9% Span a.) Close Spacing b.) Far Spacing

Figure 4.4.4: Entropy Radial Slice at 14.3% Span a.) Close Spacing b.) Far Spacing

Figure 4.4.5: Entropy Radial Slice at 17.2% Span a.) Close Spacing b.) Far Spacing
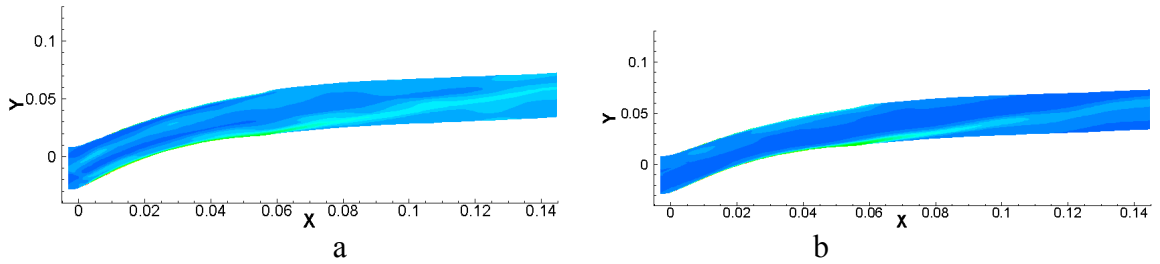
Figure 4.4.6: Entropy Radial Slice at 20.5% Span a.) Close Spacing b.) Far Spacing
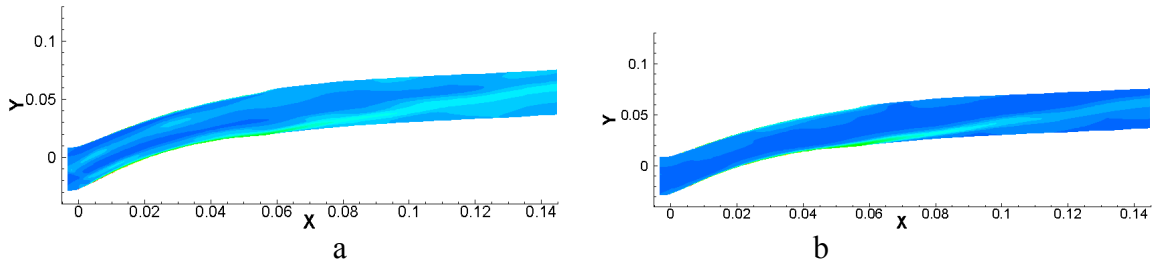
Figure 4.4.7: Entropy Radial Slice at 23.5% Span a.) Close Spacing b.) Far Spacing
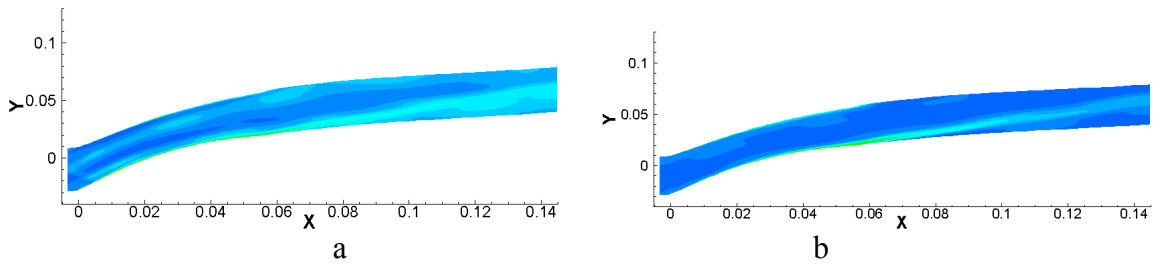
Figure 4.4.8: Entropy Radial Slice at 27.6% Span a.) Close Spacing b.) Far Spacing
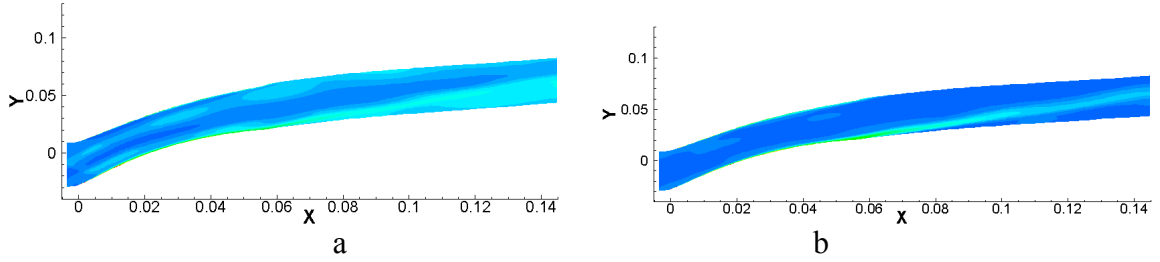
Figure 4.4.9: Entropy Radial Slice at 31.4% Span a.) Close Spacing b.) Far Spacing
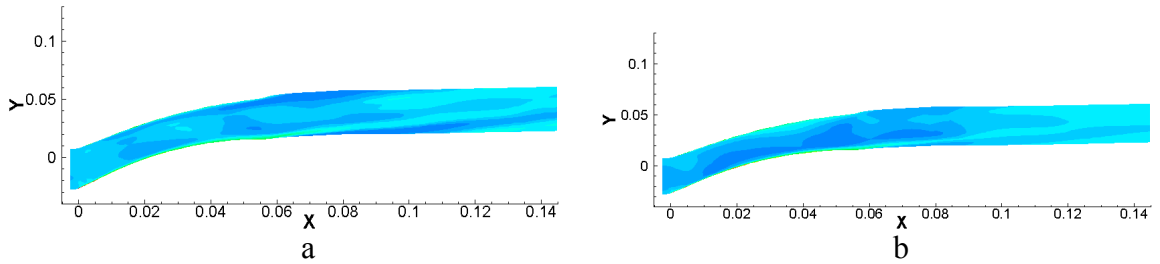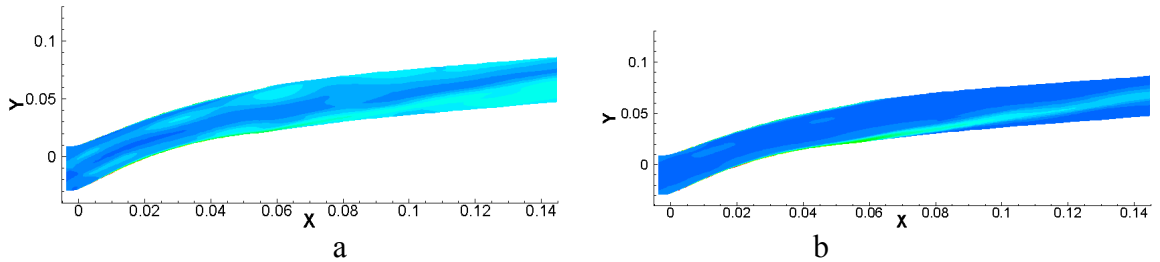

Figure 4.4.10: Entropy Radial Slice at 35.3% Span a.) Close Spacing b.) Far Spacing
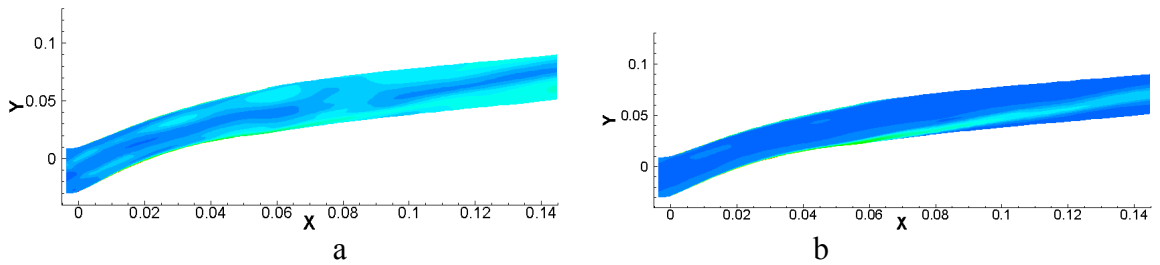
Figure 4.4.11: Entropy Radial Slice at 39.4% Span a.) Close Spacing b.) Far Spacing
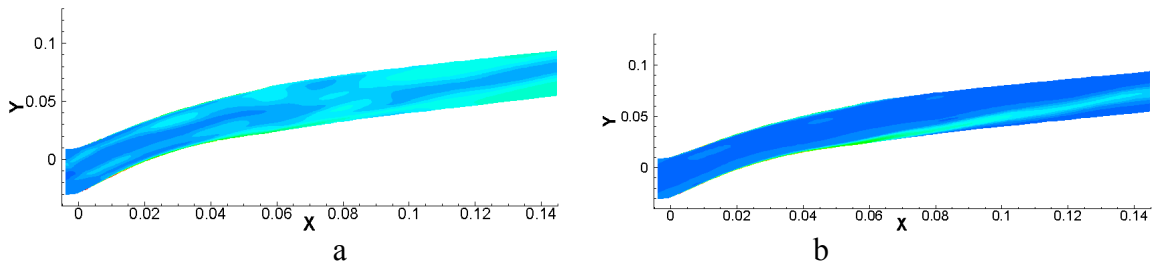
Figure 4.4.12: Entropy Radial Slice at 43.5% Span a.) Close Spacing b.) Far Spacing
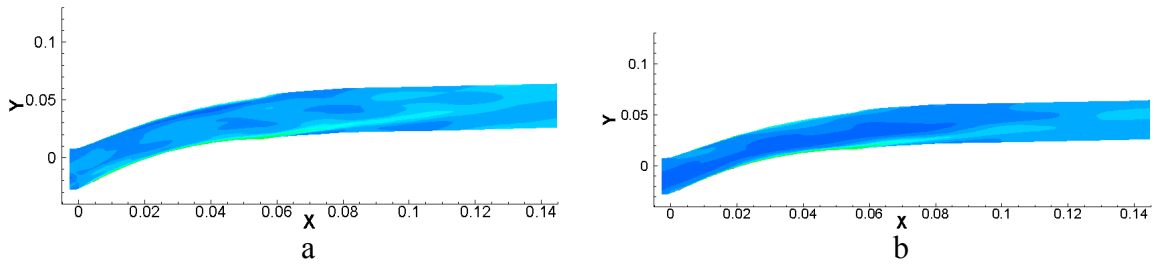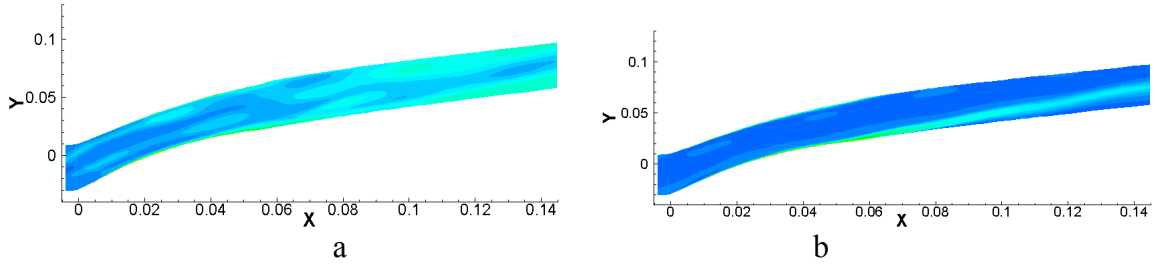
Figure 4.4.13: Entropy Radial Slice at 47.6% Span a.) Close Spacing b.) Far Spacing
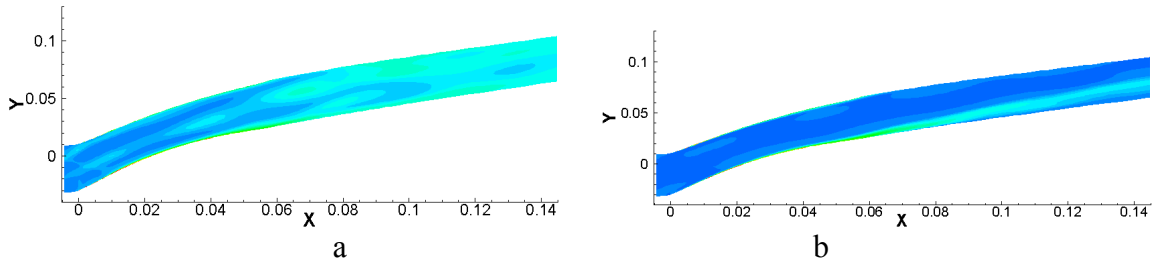
Figure 4.4.14 Entropy Radial Slice at 55.8% Span a.) Close Spacing b.) Far Spacing
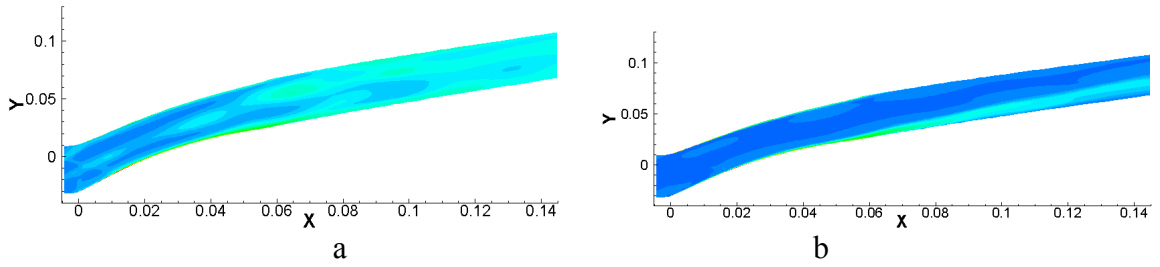
Figure 4.4.15: Entropy Radial Slice at 59.7% Span a.) Close Spacing b.) Far Spacing
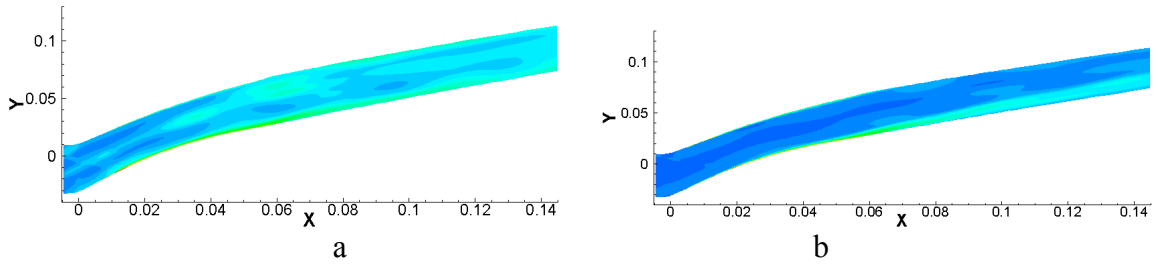
Figure 4.4.16: Entropy Radial Slice at 67.1% Span a.) Close Spacing b.) Far Spacing
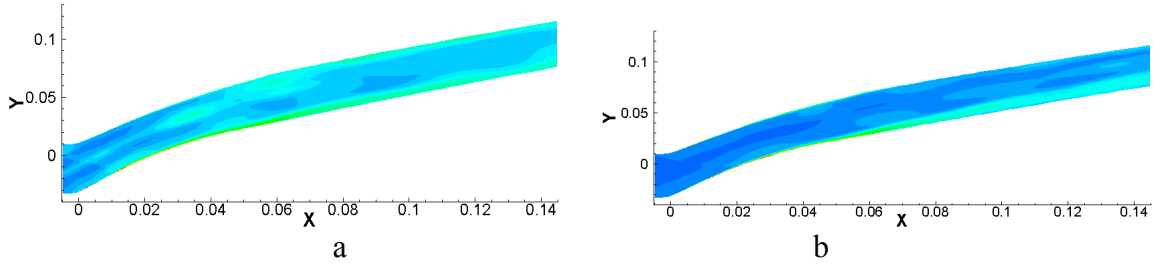
Figure 4.4.17: Entropy Radial Slice at 70.4% Span a.) Close Spacing b.) Far Spacing
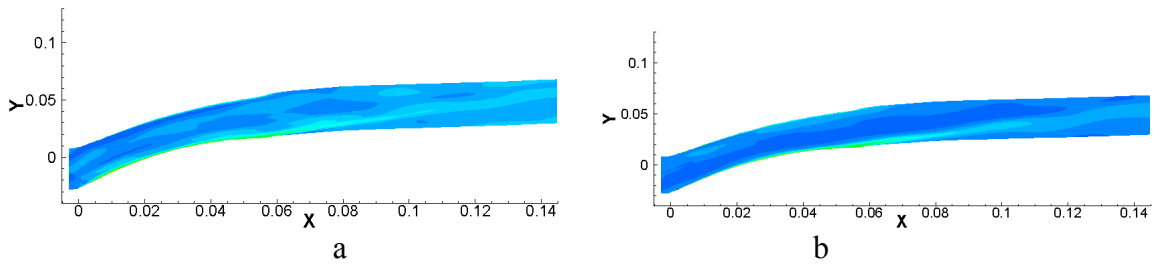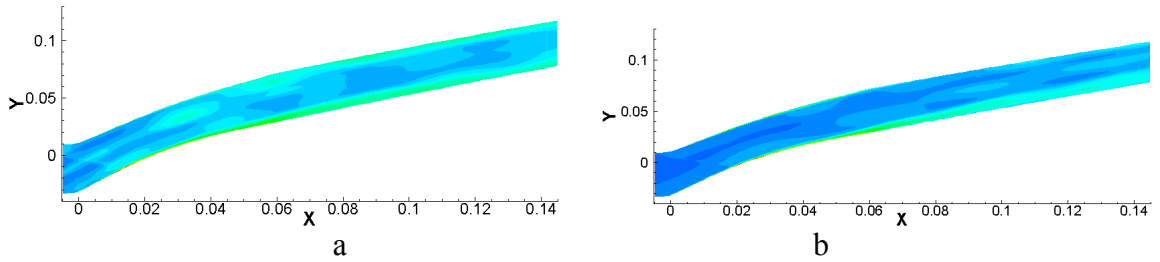

Figure 4.4.18: Entropy Radial Slice at 73.5% Span a.) Close Spacing b.) Far Spacing
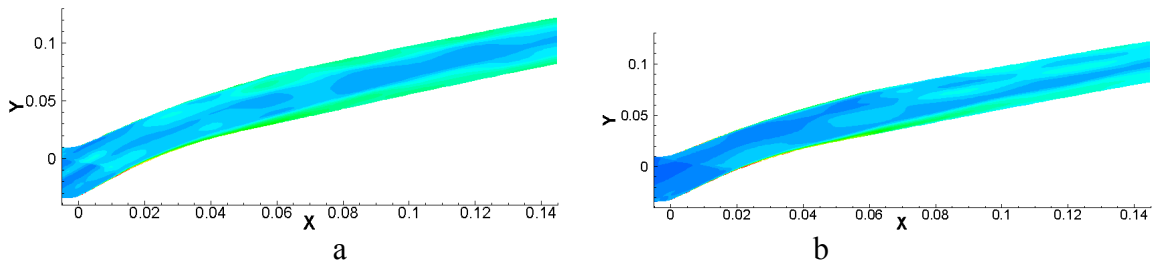
Figure 4.4.19: Entropy Radial Slice at 81.5% Span a.) Close Spacing b.) Far Spacing
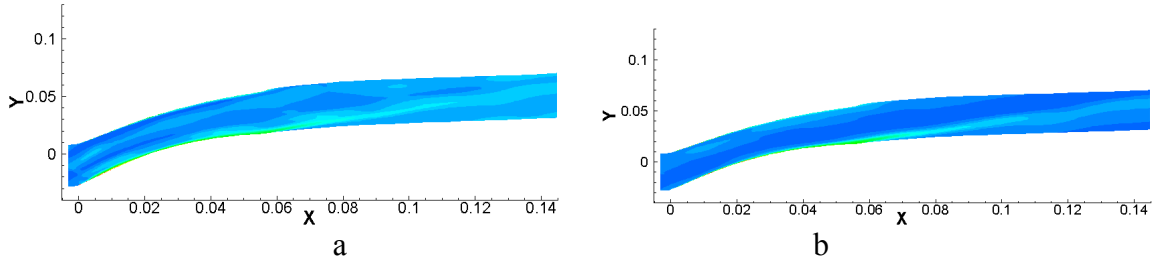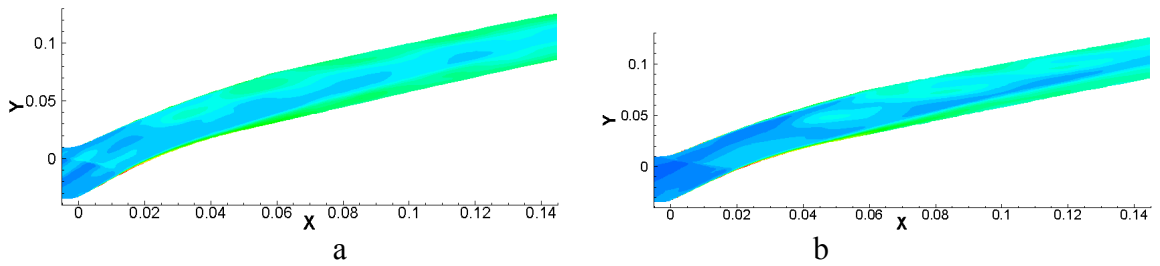

Figure 4.4.20: Entropy Radial Slice at 87.4% Span a.) Close Spacing b.) Far Spacing
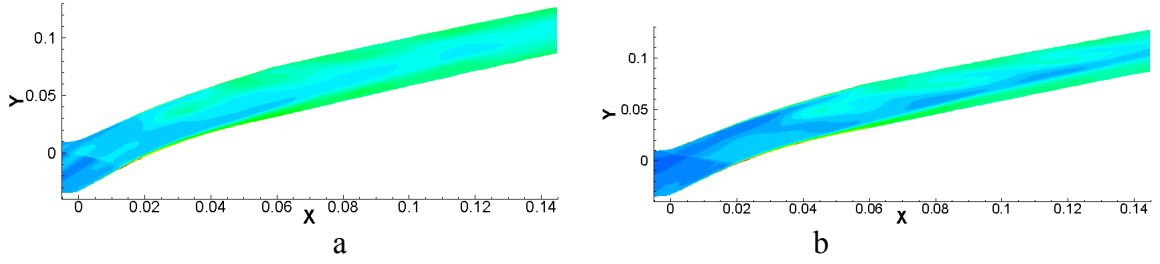
Figure 4.4.21: Entropy Radial Slice at 89.0% Span a.) Close Spacing b.) Far Spacing
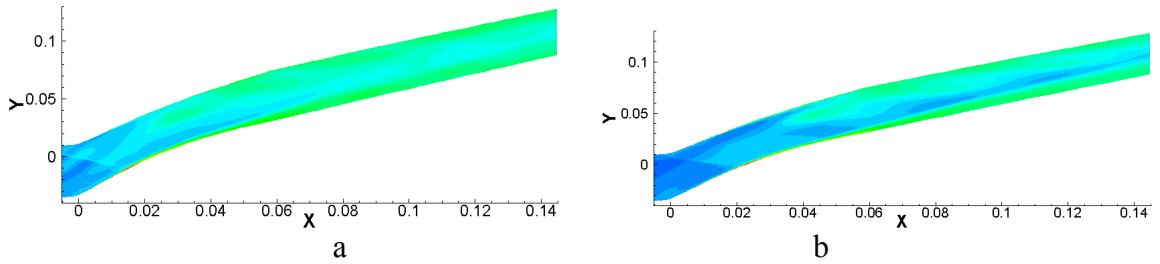
Figure 4.4.22: Entropy Radial Slice at 90.3% Span a.) Close Spacing b.) Far Spacing
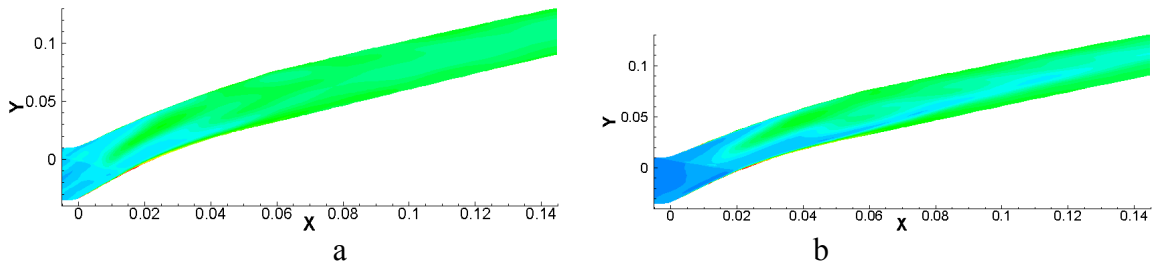
Figure 4.4.23: Entropy Radial Slice at 94.4% Span a.) Close Spacing b.) Far Spacing
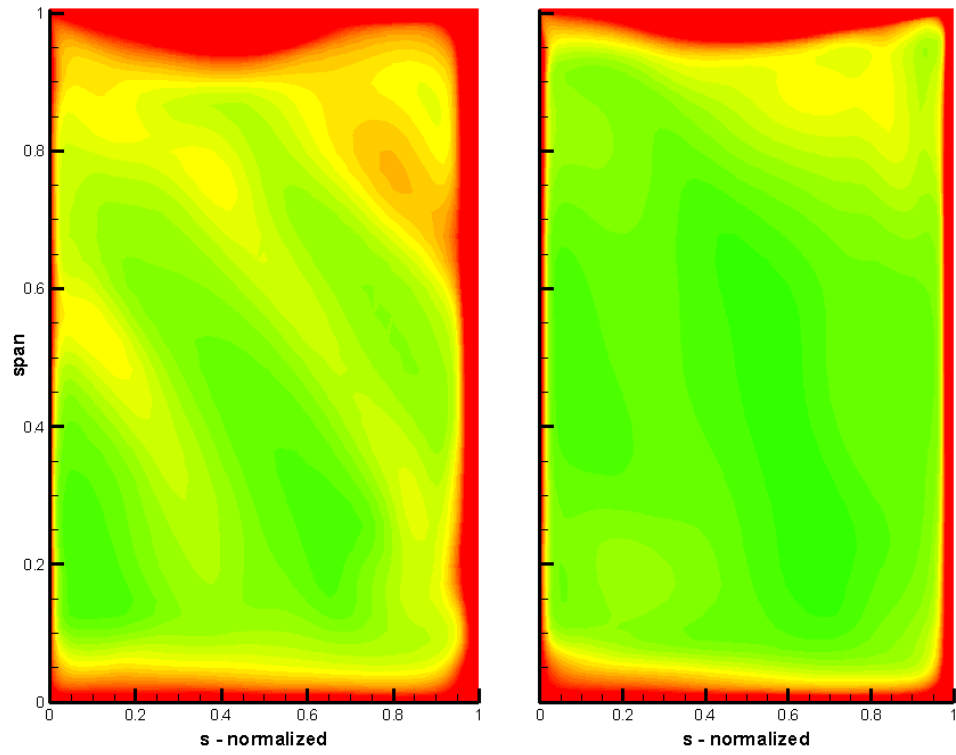
Figure 4.5.1: Entropy Axial Slice for Close and Far at 25.00% Chord
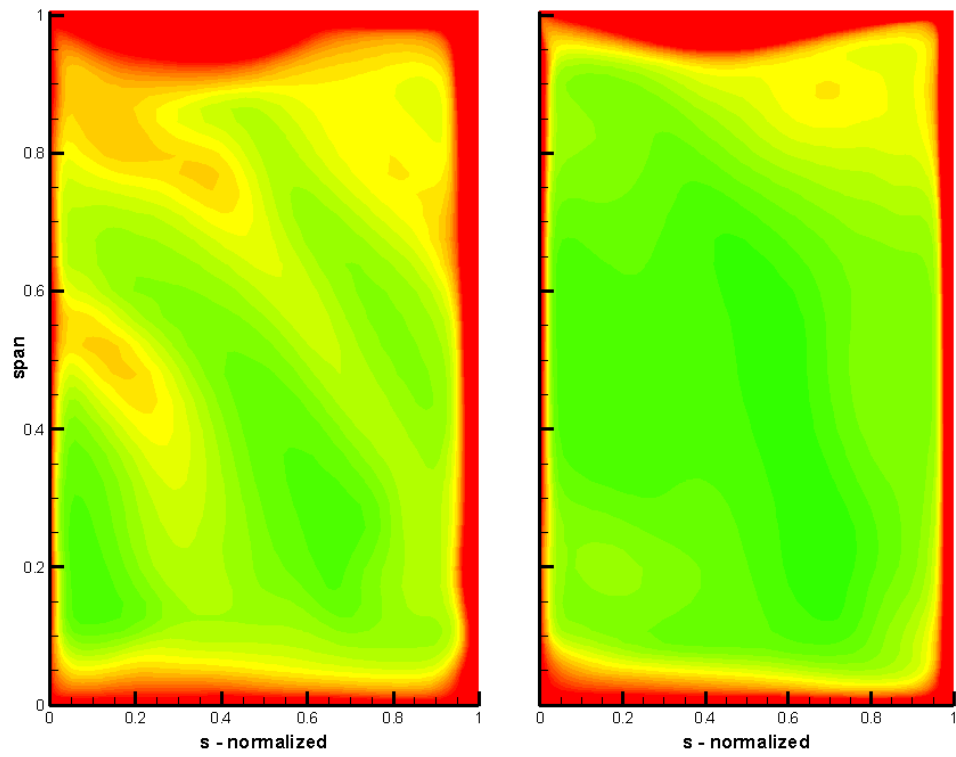
Figure 4.5.2: Entropy Axial Slice for Close and Far at 31.25% Chord

43
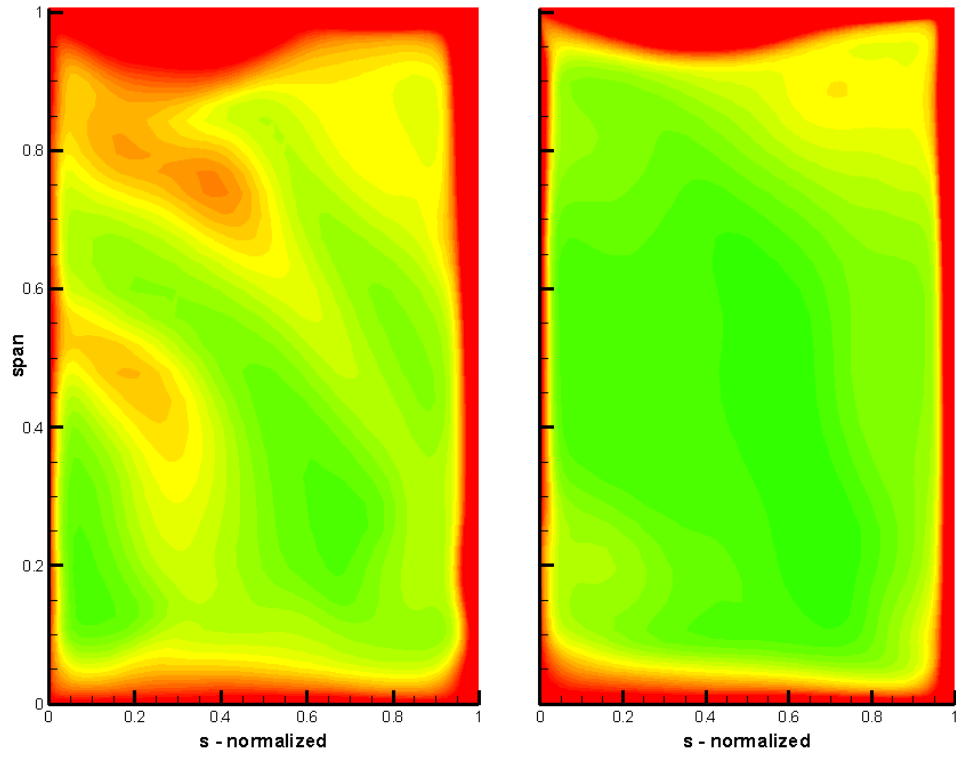
Figure 4.5.3: Entropy Axial Slice for Close and Far at 37.50% Chord
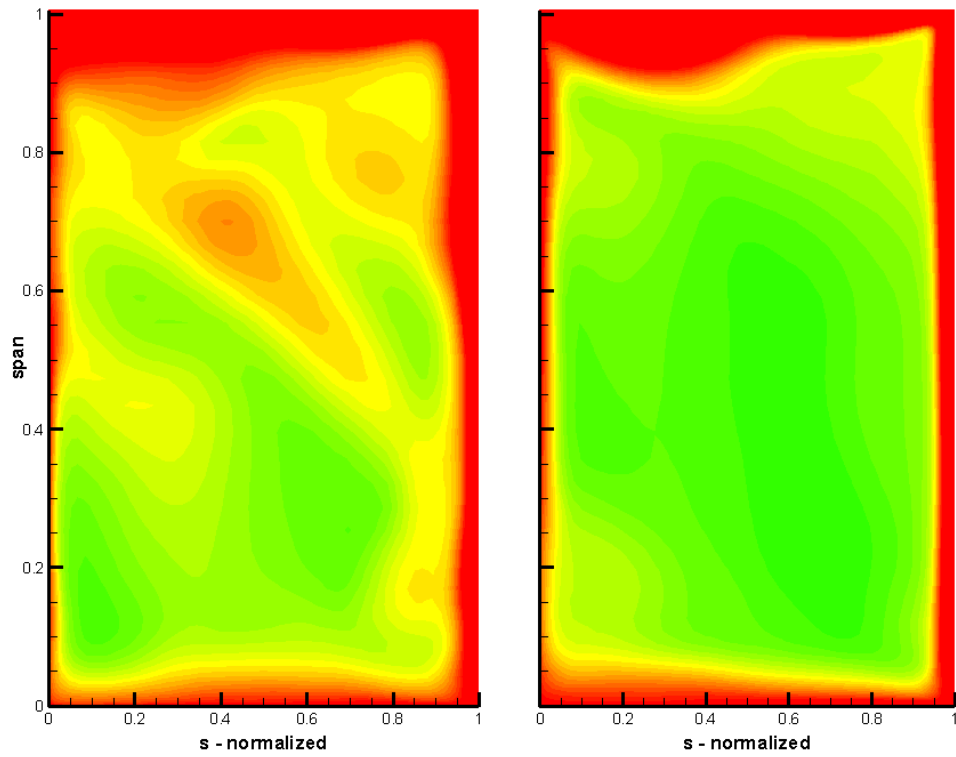
Figure 4.5.4: Entropy Axial Slice for Close and Far at 56.25% Chord
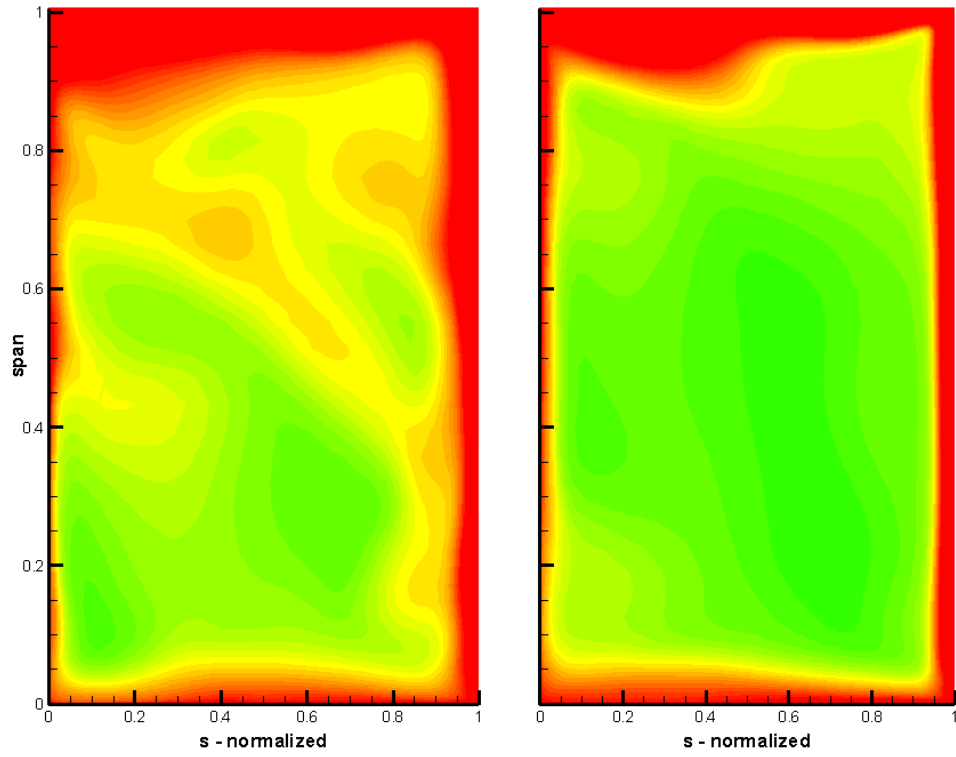
Figure 4.5.5: Entropy Axial Slice for Close and Far at 62.50% Chord
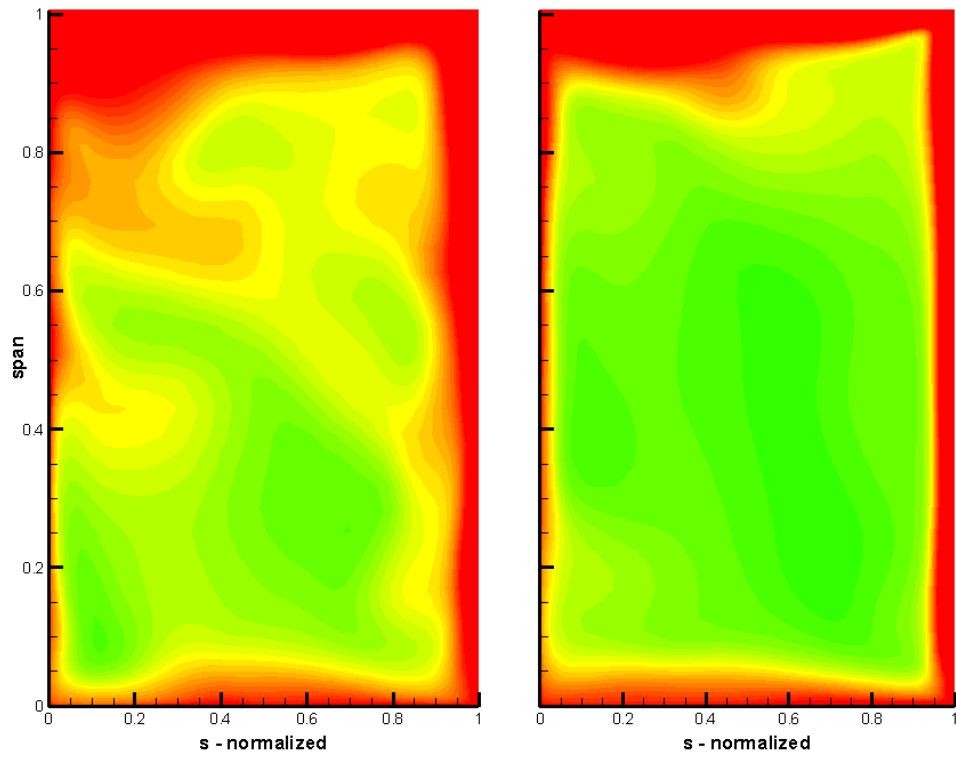
Figure 4.5.6: Entropy Axial Slice for Close and Far at 68.75% Chord

45
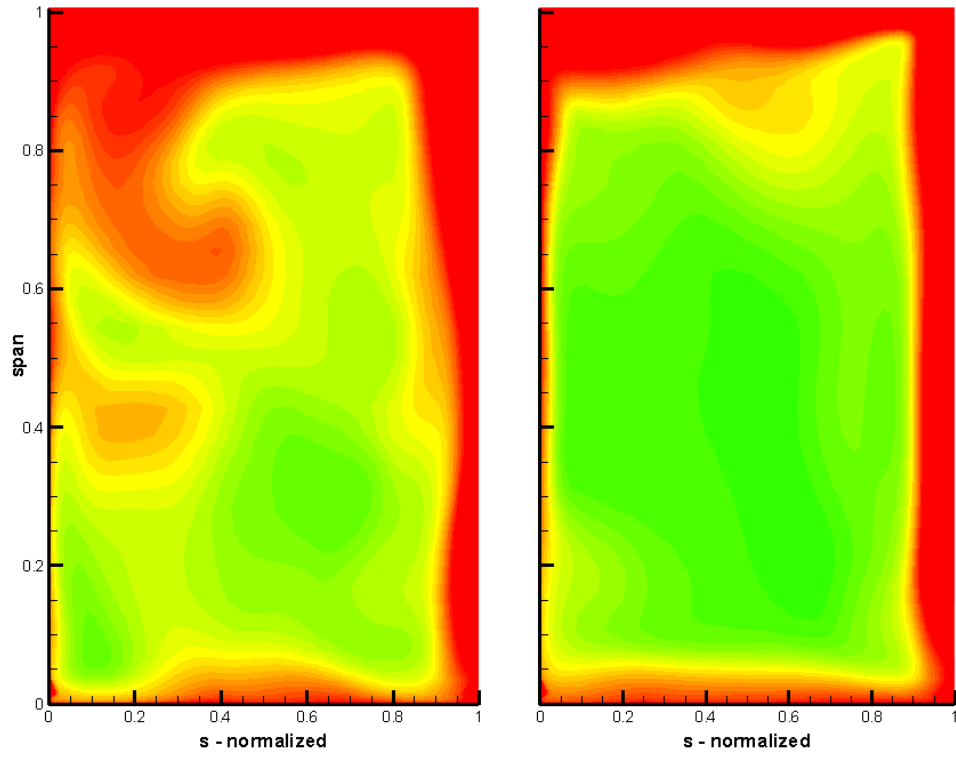
Figure 4.5.7: Entropy Axial Slice for Close and Far at 81.25% Chord
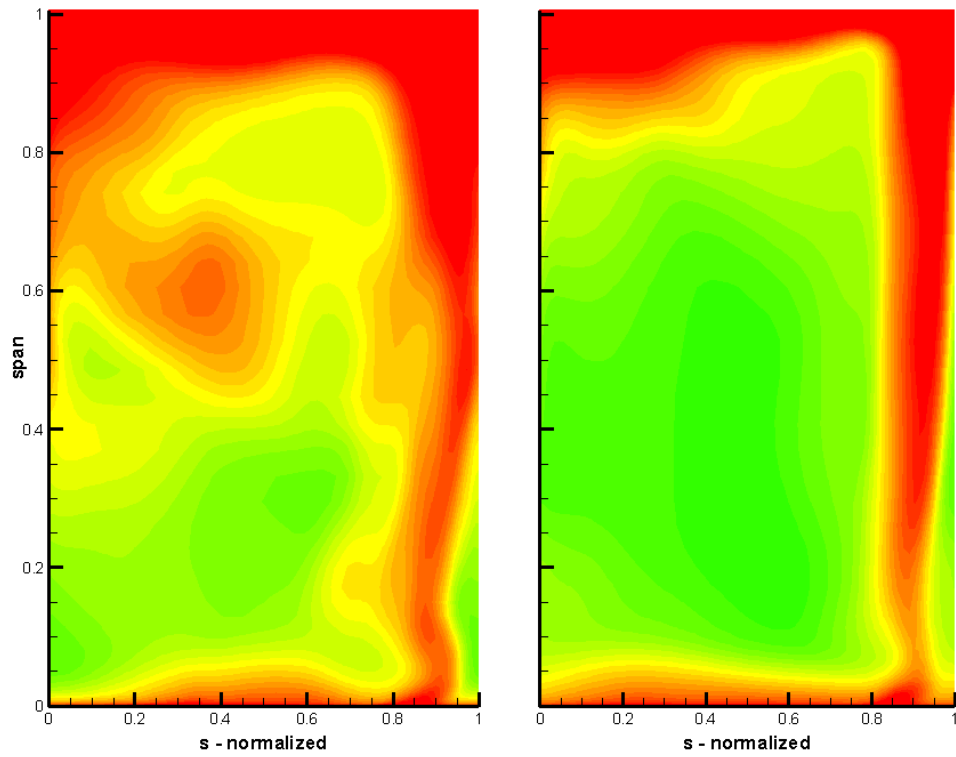
Figure 4.5.8: Entropy Axial Slice for Close and Far at 100.00% Chord

46
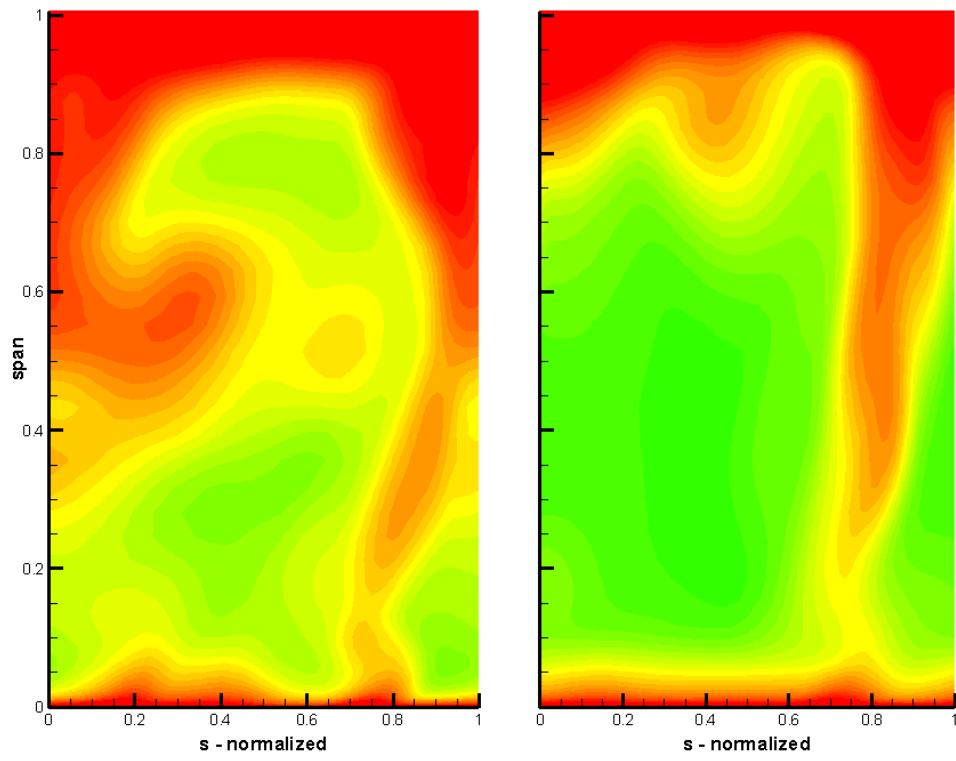
Figure 4.5.9: Entropy Axial Slice for Close and Far at 131.25% Chord

Appendix C: Input Files

APG User Guide

A primary directory for APG is created and named "/apg". All APG files and sub-directories need to be placed in the primary directory. All APG scripts use the master file "default_data.info" to control parameters associated with grid density, spacing, clearance size, etc. The file "axi.inp" is place in a sub-directory "/apg/axi" and is used to generate the axisymmetric grid. The sub-directories "/apg/blade1" and "/apg/blade2" are created for the scripts "trim.inp" and "grid.inp", a copy of each should be placed in each sub-directory.   The script "trim.inp" is used to trim the axisymmetric gird, while the script "grid.inp" creates a 3D grid file. The APG executable file "apg6f.x" should be placed in all sub-directories.

The geometry is defined in six files placed in the sub-directory "/apg/geometry". The geometry files are called by the scripts, "*.inp". The six geometry files are: hub line, casing line, inlet plane, exit plane, blade1, and blade2. Each file is discussed below.

Hub Line: A *.dat file containing three columns (x,r,θ) of non-dimensional (non-dimensionalized by the rig diameter) data defining the axisymmetric characteristics of the hub from the inlet to exit of the modeled blade rows. The file header is composed of two lines: a generic file name and the integer number of (x,r,θ) locations.

Casing Line: A *.dat file containing three columns (x,r,θ) of non-dimensional (non-dimensionalized by the rig diameter) data defining the axisymmetric characteristics of the

casing from inlet to exit of the modeled blade rows. The file header is composed of two lines: a generic file name and the integer number of (x,r,θ) locations.

Inlet Plane: A *.dat file containing three columns (x,r,θ) of non-dimensional (non-dimensionalized by the rig diameter) data defining the axisymmetric characteristics of the inlet to the modeled blade rows. At least four (x,r,θ) points are required. The file header is composed of two lines: a generic file name and the integer number of (x,r,θ) locations.

Exit Plane: A *.dat file containing three columns (x,r,θ) of non-dimensional (non-dimensionalized by the rig diameter) data defining the axisymmetric characteristics of the exit to the modeled blade rows. At least four (x,r,θ) points are required. The file header is composed of two lines: a generic file name and the integer number of (x,r,θ) locations.

Blade1: A *.fmt formatted PLOT3D file containing blocks of non-dimensional (non-dimensionalized by the rig diameter) x, y, and z data defining the Cartesian geometry of the first blade-row blade. Data are written in a specific order relative to the blade: starting at the blade trailing edge at one radial location, moving forward to the leading edge, and then back to the trailing edge on the other blade surface. This order must be repeated at over at least five radial locations (moving from hub to casing) to define the span-wise variation of the blade. The file header is composed of one line containing three numbers: the number of data points at each radial location, the number of radial locations, and number of blocks. The wake generator geometry is defined in Blade1 file.

Blade2: A *.fmt formatted PLOT3D file containing blocks of non-dimensional (non-dimensionalized by the rig diameter) x, y, and z data defining the Cartesian geometry of the second blade-row blade. Data are written in a specific order relative to the blade: starting at the blade trailing edge at one radial location, moving forward to the leading edge, and then back to the trailing edge on the other blade surface. This order must be repeated at over at least five radial locations (moving from hub to casing) to define the span-wise variation of the blade. The file header is composed of one line containing three numbers: the number of data points at each radial location, the number of radial locations, and number of blocks. The rotor blade geometry is defined in the Blade2 file.

After the grid files are defined, the grid can be created. Generating the grid is done by executing the script "apg.inp" via the command "apg6f.x –s axi.inp" at a UNIX command prompt (the flag "-s" signals APG to run the subsequently named scripts). The process of creating the axisymmetric grid consists of the following steps:

1. Definition of input file location

2. Initialization of grid

3. Input of data files

4. Definition of hub, casing, inlet, and exit curves

5. Definition of IGV (blade1) and rotor (blade2) surfaces

6. Extension of blade hub and tip locations beyond hub and casing curves

7. Creation of axisymmetric grid

8. Splitting of axisymmetric grid at blade1/blade2 interface location

9. Output of axisymmetric grid files

Once the grid is generated, the following steps are used to trim each blade row:

1. Definition of input file locations and trimming tolerance

2. Initialization of the grid

3. Input of the data files

4. Extension of blade hub and tip locations beyond hub and casing curves

5. Definition of IGV (blade1), or rotor (blade2), surface

6. Trimming of axisymmetric grid

7. Output of trimmed grid files

The grid generation can begin after the trimming process has been completed. The 3D grid is constructed by following the steps below:

1. Definition of input file locations and trimming tolerance

2. Initialization of the grid

3. Input of the data files

4. Extension of blade hub and tip locations beyond hub and casing curves

5. Definition of IGV (blade1), or rotor (blade2), surface grid properties

6. Creation of IGV (blade1), or rotor (blade2), surface grid

7. Creation of 3D grid

8. Output of 3D grid files

If the directories, sub-directories, data files, and scripts are position appropriately, then the following tasks (starting from the primary directory) must be performed to complete the blade1 and blade2 3D grids. Depending on the size of the grid, several minutes ay be required for each execution of "apg6f.x", noting that the script "trim.inp" will require the most computational time and resources.

- UNIX: cd axi

- UNIX: apg6f.x –s axi.inp

- UNIX: cd ..\blade1

- UNIX: apg6f.x –s trim.inp

- UNIX: apg6f.x –s grid.inp

- UNIX: cd ..\blade2

- UNIX: apg6f.x –s trim.inp

- UNIX: apg6f.x –s grid.inp

Execution of the above commands at the UNIX prompt will produce several output data files in each sub-directory named "apg/blade1" and "apg/blade2". Files of importance to MSU-TURBO include the VSTAGE formatted output grids "m01.d" and "m02.d" for blade1 and blade2, respectively; as well as the PLOT3D formatted output grids "igv.fmt" and "rotor.fmt" for blade1 and blade2, respectively. VSTAGE formatted grid files are of particular importance, as these files (when included with appropriate *.info files) contain the appropriate boundary conditions for each blade row (Falk, 2003).

APG Text Input Files

Blunt-IGV, Sharp-IGV, and Rotor (default_data.txt)

/---

        This file contains the default griding parameters
           for APG. You can change the default and it will
           override the parameters that are in the APG
           script files.

           NOTE: In the parameters below
        a positive number for spacing is nondimensionalized by
        the span or the chord length, while a negative number
        is in physical units. Axial spacing on the blade is
        only nondimensionalized by the chord length.

/---------- Default Parameters For Axisymmetric Grid ----------------------

```
#DEFINE PRECISION single
#DEFINE REF 1.0                          ! reference length
#DEFINE DZ_HUB_IN 0.050                  ! axial spacing at the inlet of axi grid near the hub
#DEFINE DZ_HUB_OUT 0.050                 ! axial spacing at the outlet of axi grid near the hub
#DEFINE DR_HUB_IN 0.002                  ! radial spacing at inlet of axi grid near the hub
#DEFINE DR_HUB_OUT 0.008                 ! radial spacing at the outlet of axi grid near the hub
#DEFINE DZ_TIP_IN 0.050                  ! axial spacing at the inlet of axi grid near the tip
#DEFINE DZ_TIP_OUT 0.050                 ! axial spacing at the outlet of axi grid near the tip
#DEFINE DR_TIP_IN 0.002                  ! radial spacing at inlet of axi grid near the tip
#DEFINE DR_TIP_OUT 0.002                 ! radial spacing at the outlet of axi grid near the tip
#DEFINE DR_LE 0.002                      ! radial spacing at the blade leading edge of axi grid
#DEFINE DR_TE 0.002                      ! radial spacing at the blade trailing edge of axi grid
#DEFINE NSPAN 70                         ! number of radial
#DEFINE SPANWISE_AXI 1,21,31,41,51,61! spanwise location to perform smoothing of axi grid
```

/ Data for Blade 1

```
#DEFINE MNXI 0                           ! number of cells in inlet rectifying cell, 0 will set it to 1/2 of
                                           total cell in gap
#DEFINE MDXI 0.0                         ! axial grid spacing at inlet rectifying cell, nondimensionalized
                                           by spacing at following trailing edge
#DEFINE MARCI 0.0                        ! inlet rectifying cell location along curve between trailing
                                           edge and leading edge(0.5 is midpoint)

#DEFINE NX_I 10                           ! number of axial points at the inlet of axi grid
#DEFINE NX_B1 40                         ! number of axial points on the blade of axi grid
#DEFINE DS_LE_AXI1 0.004                 ! axial spacing at the blade leading edge of axi grid
#DEFINE DS_TE_AXI1 0.004                 ! axial spacing at the blade trailing edge of axi grid
#DEFINE OFFSET11 2                       ! grid offset at the inlet of axi grid
#DEFINE OFFSETR11 0.2                    ! grid offset at the inlet of axi grid
#DEFINE OFFSET21 -2                      ! grid offset at the outlet of axi grid
#DEFINE OFFSETR21 0.2                    ! grid offset at the outlet of axi grid
#DEFINE ROOFTOP1 0                       ! number of cells in the rooftop
#DEFINE ROOFSIZE1 0.000                  ! size of the rooftop as a 46431250f tipclearance
#DEFINE MNXG1 10                         ! number of cells before rectifying cell, 0 will set it to 1/2 of
                                           total cell in gap
```

```
#DEFINE MDXG1 2.                        ! axial grid spacing at rectifying cell, nondimensionalized by
                                        spacing at following trailing edge
#DEFINE MARCG1 0.6453                   ! rectifying cell location along curve between trailing edge and
                                        leading edge(0.5 is midpoint)


/ Data for Blade 2

#DEFINE NX_G1 17                        ! number of axial points in gap between b1 & b2
#DEFINE NX_B2 40                        ! number of axial points on the blade of axi grid
#DEFINE NX_O 44                         ! number of axial points at the outlet of axi grid
#DEFINE DS_LE_AXI2 0.004                ! axial spacing at the blade leading edge of axi grid
#DEFINE DS_TE_AXI2 0.004                ! axial spacing at the blade trailing edge of axi grid
#DEFINE OFFSET122 2                     ! grid offset at the inlet of axi grid
#DEFINE OFFSETR12 0.2                   ! grid offset at the inlet of axi grid
#DEFINE OFFSET22 -2                     ! grid offset at the outlet of axi grid
#DEFINE OFFSETR22 0.2                   ! grid offset at the outlet of axi grid
#DEFINE ROOFTOP2 0                      ! number of cells in the rooftop
#DEFINE ROOFSIZE2 0.000                 ! size of the rooftop as a 46431250f tipclearance
#DEFINE MNXO 20                         ! number of cells in outlet rectifying cell, 0 will set it to 1/2 of
                                        total cell in gap
#DEFINE MDXO 8.                         ! axial grid spacing at outlet rectifying cell,
                                        nondimensionalized by spacing at following trailing edge
#DEFINE MARCO 0.300                     !  outlet rectifying cell location along curve between trailing
                                        edge and leading edge(0.5 is midpoint)


/---------- Default Parameters For 3D Grid -------------------------------

/ Data for Blade 1

#DEFINE DS_LE1 0.002                    ! axial spacing at the blade leading edge of 3D grid, not used
                                        when leading edge points is >0
#DEFINE DS_TE1 0.002                    ! axial spacing at the blade trailing edge of 3D grid
#DEFINE BLADE_POINTS1 80                ! number of axial points on the blade of 3D grid
#DEFINE DSIN1 0.050                     ! axial spacing at the inlet of 3D grid
#DEFINE DSOUT1 0.050                    ! axial spacing at the outlet of 3D grid
#DEFINE DTIN1 0.01                      ! tangential spacing at the inlet of 3D grid
#DEFINE DTOUT1 0.0045                   ! tangential spacing at the outlet of 3D grid
#DEFINE WALLSPACING1 0.500              ! wall spacing
#DEFINE SPANWISE_3D1 1,7,11,21,31,41,51,61,65,71 ! spanwise location to perform smoothing of 3D
                                        grid
#DEFINE CELLS_THETA1 60                 ! number of cells blade to blade
#DEFINE NFRONT1 20                      ! number of cells before the blade in the 3D grid
#DEFINE NBACK1 17                       ! number of cells after the blade in the 3D grid
#DEFINE LEADING_EDGE_POINTS1 10 ! number of blade leading edge points in the 3D grid
#DEFINE TRAILING_EDGE_POINTS1 30 ! number of blade trailing edge points in the 3D grid
#DEFINE TIPCELLS1 8                     ! number of cells in the tip clearance
#DEFINE TIPCLEARANCE1 0.000789474  ! Physical tip clearance
#DEFINE TIPPACKING1 0.2                 ! radial spacing intip clearance at blade ndim by clearance
#DEFINE ROOFTOP1 0                      ! number of cells in the rooftop
#DEFINE ROOFSIZE1 0.000                 ! size of the rooftop as a % of tipclearance
#DEFINE A_GRAPE1 0.600                  ! grape coefficient
#DEFINE B_GRAPE1 0.600                  ! grape coefficient
#DEFINE C_GRAPE1 0.600                  ! grape coefficient
#DEFINE D_GRAPE1 0.600                  ! grape coefficient
#DEFINE DMLE1 0.500                     ! control parameter for L.E cut location
#DEFINE DMTE1 0.900                     ! control parameter for T.E cut location
```

```
#DEFINE LEOFFSET1 0.300              ! control parameter for L.E periodic line
#DEFINE TEOFFSET1 1.000              ! control parameter for T.E periodic line
#DEFINE NUMIT1 200                   ! control parameter for number of grape iterations


/ Data for Blade 2

#DEFINE DS_LE2 0.002                 ! axial spacing at the blade leading edge of 3D grid, not used
                                       when leading edge points is >0
#DEFINE DS_TE2 0.002                 ! axial spacing at the blade trailing edge of 3D grid
#DEFINE BLADE_POINTS2 80             ! number of axial points on the blade of 3D grid
#DEFINE DSIN2 0.050                  ! axial spacing at the inlet of 3D grid
#DEFINE DSOUT2 0.050                 ! axial spacing at the outlet of 3D grid
#DEFINE DTIN2 0.005                  ! tangential spacing at the inlet of 3D grid
#DEFINE DTOUT2 0                     ! tangential spacing at the outlet of 3D grid
#DEFINE WALLSPACING2 0.500           ! wall spacing
#DEFINE SPANWISE_3D2 1,2,3,4,5,11,21,31,41,51,61      ! spanwise location to perform smoothing of
                                       3D grid
#DEFINE CELLS_THETA2 80              ! number of cells blade to blade
#DEFINE NFRONT2 18                   ! number of cells before the blade in the 3D grid
#DEFINE NBACK2 90                    ! number of cells after the blade in the 3D grid
#DEFINE LEADING_EDGE_POINTS2 10 ! number of blade leading edge points in the 3D grid
#DEFINE TRAILING_EDGE_POINTS2 20 ! number of blade trailing edge points in the 3D grid
#DEFINE TIPCELLS2 8                  ! number of cells in the tip clearance
#DEFINE TIPCLEARANCE2 0.000789474 ! Physical tip clearance
#DEFINE TIPPACKING2 0.015            ! radial spacing intip clearance at blade ndim by clearance
#DEFINE ROOFTOP2 0                   ! number of cells in the rooftop
#DEFINE ROOFSIZE2 0.000              ! size of the rooftop as a % of tipclearance
#DEFINE A_GRAPE2 0.600               ! grape coefficient
#DEFINE B_GRAPE2 0.600               ! grape coefficient
#DEFINE C_GRAPE2 0.600               ! grape coefficient
#DEFINE D_GRAPE2 0.600               ! grape coefficient
#DEFINE DMLE2 0.700                  ! control parameter for L.E cut location
#DEFINE DMTE2 0.900                  ! control parameter for T.E cut location
#DEFINE DELTALECUT2 20.000           ! control parameter for L.E. cut location angle (in deg)
#DEFINE DELTATECUT2 0.000            ! control parameter for T.E. cut location angle (in deg)
#DEFINE LEOFFSET2 0.300              ! control parameter for L.E periodic line
#DEFINE TEOFFSET2 1.000              ! control parameter for T.E periodic line
#DEFINE NUMIT2 400                   ! control parameter for number of grape iterations

END OF INPUT
```

MSU-TURBO Text Input Files

The files required by MSU-TURBO are as follows:

- bc.in: Input text file containing boundary conditions for each grid block. This file must be present in the same directory from which MSU-TURBO is executed.

The file is output directly from GUMBO when the "-GU" command is invoked while saving the grid file.

- dmap.in: Input text file containing information about block-to-block connectivity. This file must be present in the same directiory from which MSU-TURBO is executed. The file is output directly form GUMBO when the "-GU" command is invoked while saving the grid file.

- turbo.in: Input text containing information about sliding-mesh interface connectivity. This file much be present in the same directory from which MSU-TURBO is executed. The file is output directly from GUMBO when the "-GU" command is invoked while saving the grid file.

- input00: Input text file containing parameters for MSU-TURBO flow solver, such as: number of blade rows, initial solution conditions, reference conditions, turbulence model variables, time-step/CFL definitions, output format, etc. This file is not output by GUMBO, but can be created via the MSU-TURBO user interface/GUI. An example code for the Input00 file is provided below. Note that "*" denotes a comment not included in the actual file and "[…]" indicates the default value for each parameter.

Further information can be found in the research by Falk (2003).

Input00.txt

```
&PARAMETERS                              *Begin parameter namelist
num_blade_rows = 2                       *Specify number of blade rows in simulation
debug = F                                *Turns debug flaf on (T) or off (F)
gofast = T
/

&SOLUTION_PARAMETERS                     *Begin solution parameters namelist
num_printouts = 1                        *# of printouts
num_iter_per_printout = 270              *# of iterations per printout
```

```
max_num_subiter = 6                          *# of sub-iterations per time step
num_sgs_iter = 3                             *#of Gauss-Seidel passes for each sub-iteration
freeze_jacobian = 0                          *Jacobian freeze on (1)/ off (0)
num_iter_without_fluxfix = 0
num_iter_inviscid = 0
num_iter_first_order = 0
num_iter_restart_write = 270
num_iter_zero_grad_bc = 0
temporal_accuracy = 2
spatial_accuracy = 3
limiter_flag = 1
solution_type = 2
turbulence_model = 5
symmetry_factor=0
trap_negative = F
/

&SLIDING_BC
use_conserve_bc = 0
/

&INITIAL_CONDITION
initialize_solution = 4
/

&REFERENCE_CONDITIONS
ref_length = 0.4826
ref_gamma = 1.401290
ref_pressure = 101325.00
ref_temperature = 288.150
ref_velocity = 287.567
gamma_table = 1.401290 1.401290
temp_gam_table = 288.15 388.15
gamref_t1 = 1.401290
/

&ke_MODEL_PARAMETERS
kemdl_input_type = 0
kemdl_init_option = 0
spatial_accuracy_2eq = 3
temporal_accuracy_2eq =  2
inlet_turbulence_intensity = 0.02
inlet_eddy_viscosity = 10.
use_pgrad_term = F
/

&TIME_SHIFT_BC
time_shift_bc_factor = 0.5
use_time_shift_bc = 1
initialize_time_shift_in_TURBO = T
/

&INLET_BC
inlet_bc_type = -2
/
```

&EXIT_BC
exit_bc_type = -1
back_pressure = 117243.27934
/

&FLUTTER
/

&TIME_STEP
cfl = 0.0
use_local_time_step = 0
num_time_steps_per_period = 270
omega_ts = -13509.0
num_blds_ts = 33
/

&OUTPUT
num_soln_per_flow_file = 3
num_iter_per_soln_dump = 9
output_format = 1
/

&INLET_PROFILE
span =
0.000685233
0.002739052
0.006155830
0.010926200
0.017037087
0.024471742
0.033209787
0.043227271
0.054496738
0.080664716
0.111427019
0.146446609
0.185339804
0.227680482
0.273004750
0.320816025
0.370590477
0.421782767
0.473832022
0.526167978
0.578217233
0.629409523
0.679183975
0.726995250
0.772319518
0.814660196
0.853553391
0.888572981
0.919335284
0.933012702
0.945503262
0.956772729

0.966790213
0.975528258
0.982962913
0.989073800
0.993844170
0.997260948
0.999314767

total_pressure =
86614.79847
89940.10803
92625.07588
94911.93001
96876.55497
98539.31041
99891.95562
100904.8672
101525.5682
101684.2879
101684.2879
101684.2879
101684.2879
101684.2879
101684.2879
101684.2879
101684.2879
101684.2879
101684.2879
101684.2879
101684.2879
101684.2879
101684.2879
101684.2879
101684.2879
101684.2879
101684.2879
101684.2879
101684.2879
101684.2879
101684.2879
101476.4004
100551.563
99028.76147
96994.19349
94475.3091
91422.43561
87588.80382

total_temperature =
39*288.15

tangential_angle =
39*0.0

radial_angle =

39*0.0

turbulence_intensity =
39*0.02

turbulence_length_scale =
39*0.001
/

&EXIT_PROFILE
/

Input01.txt

&BLADE_ROW_PARAMETERS
num_blades = 24
omega_bld = 0.0000
num_time_steps_stored = 100
num_adjacent_blades = 33
suction_surface = 2
use_wall_func_j = 1
use_wall_func_k = 1
transition = 0.001
x_start_hub_rotation = -9999.0
x_end_hub_rotation = -9999.0
x_start_case_rotation = 9999.0
x_end_case_rotation = 9999.0
/ /

Input02.txt

&BLADE_ROW_PARAMETERS
num_blades = 33
omega_bld = -13509.0000
num_time_steps_stored = 100
num_adjacent_blades = 24
suction_surface = 2
use_wall_func_j = 1
use_wall_func_k = 1
transition = 0.01
x_start_viscous_hub = -9999.0
x_start_viscous_case = -9999.0
x_start_hub_rotation = -0.00128511960404
x_end_hub_rotation = 9999.0
x_start_case_rotation = 9999.0
x_end_case_rotation = 9999.0
/

Appendix D: MSU-TURBO Output Files

The output from the MSU-TURBO software is processed into several files, described below (Falk, 2003).

- d#0: File containing distance mapping information used for each block partition (as represented by "#0"). These files are written before the first cycle is completed in any simulation case. To save computational time, these files should be saved and used upon each restart of the solution. These files should only be removed if the grid is repartitioned.

- TURBO.#.out: Files containing convergence monitors for the mean-flow solver in each block partition (as represented by "#"). Changes in density and total energy between iterations are recorded. If these files are saved, they can be used in each solution restart with the additional convergence data appended to the end of the file for each block partition.

- ast.b#.x: PLOT3D formatted grid files written for each block partition (as represented by "b#"). These files are written after the first cycle is completed, but do not need to be employed during each solution restart.

- ast.b#.q#: PLOT3D formatted flowfield solution files written for each block partition (as represented by "b#"). These files are written out after a user-specified number of iterations (as represented by "q#), but do not need to be employed for each solution restart.

- 2eq_dq.#.hs: Files containing convergence monitoring data for the two-equation k-ε turbulence solver in each block partition (as represented by "#"). Change in the k and ε are recorded at iteration/time-step. If these files are saved, they can be used in each solution restart with additional convergence data appended to the end of the file for each block partition.

- rst_out.#0: Files containing flowfield information from each block partition (as represented by "#0") necessary to restart at job from a previous solution. Before restarting the solution, these files should be renamed to corresponding QU#0 files (e.g., rst_out.10 should be renamed QU10, etc). It is also important to save old rst_out.#0 and QU#0 files as rst_old.#0.old and QU#0.old, respectively, before solution restart.

- mslfow.hs: File containing data related to cycle number, inlet mass-flow rate, and exit mass flow rate, for each modeled blade row. If this file is saved, it can be used in each solution restart with additional mass-flow values appended. This file provides a quantitative measure of solution convergence.

- prfmce.hs: File containing data related to: cycle number, inlet mass-flow rate, outlet mass-flow rate, corrected inlet mass-flow rate, corrected outlet mass-flow rate, inlet total pressure, outlet total pressure, inlet static pressure, outlet static pressure, total pressure ratio, inlet-total to exit-static pressure ratio, inlet total temperature, outlet total temperature, total temperature ratio and efficiency. If this file is saved, it can be used in each solution restart with additional mass-flow values appended. This file provides a quantitative measure of solution convergence.

- ntropy.hs: File containing two columns of data: cycle number and inlet-exit entropy change. If this file is saved, it can be used in each solution restart with the additional mass-flow values appended. This file provides a quantitative measure of solution convergence.

- TURBO.all.out: File containing overall information related to MSU-TURBO activities. Information includes cycle number, date, and elapsed wall-clock time per iteration. If this file is saved, it can be used in each solution restart with the additional values appended.

To post-process a parallel job involving multiple block partitions MSU-TURBO provides two utilities named "msuturbo –locate" and "msuturbo –merge". Note that for these utilities to operate correctly, all GU, QU, ast.b#.c, and ast.b#.q# files must be located in the same directory as the input00, input0#, *info, and original "casename.#" files. Moreover, all file formats should be consistent (i.e., MSU-TURBO input and output files all in VSTAGE format). Entering the command "msuturbo –locate –case casename" at the UNIX prompt locates each block partition grid and relates that partition grid to the original unpartitioned grid, where "-case casename" informs MSU-TURBO to locate files related to "casename". For example, if the original grid and *.info files for GUMBO were given names "un.r1b1.vstage.g.r4" and "un.r1.info", then the case name "un" must be used for the "msuturbo –locate" and "msuturbo –merge" utilities. The "msuturbo – locate" utility creates two files: "casename.insert" and "casename.extract", which are used by the subsequent "msuturbo –merge" utility.

Entering the command "msuturbo –merge –case casename –qid 1000 –vstage" at the UNIX prompt merges all ast.b#.x and ast.b#.q# solution files associated with the case "casename" at 1000 iterations (qid = 1000), where "-vstage" must be specified if the GU and QU files were saved in VSTAGE file format. Note that an additional flag "-rel" can be added to the "msuturbo –merge" utility if the output flowfield solution is desired in the relative reference frame. Output from the "msuturbo –merge" utility will be named "casename.r#b#.vstage.g.r4", "casename.r#b#.vstage.g.r8", and "casename.r#b#.vstage.1.r4"; the former two being recombined grid files and the later a complete flowfield solution at the iteration related to "#q".

Grid and Flowfield Solution File Information

Header Information for the "un.b#r#.p3dv.g.r4" files is shown in the following chart:

Header Information	Wake Generator Grid File "un.b1r#.p3dv.g.r4"	Rotor Grid File "un.b2r#.p3dv.g.r4"
Unknown 1	28	28
Axial Nodes (imxs)	190	189
Radial Nodes (jmxs)	71	71
Transverse Nodes (kmxs)	61	81
Axial Leading Edge Node (ile)	23	19
Axial Trailing Edge Node (ite)	103	99
Radial Tip Node (jtip)	71	63
Number of Blades	24	33
Unknown 2	28	28
Number of Bytes	139080	183708

The grid information is given in blocks. Each block gives the axial and transverse grid information for one radial node location. The code used to extract the flow information is as follows:

```
              DO 50 j=1,jmxs
                      READ(iunit) num_bytes
                      READ(iunit) ((     x(i,j,k),i=1,imxs),k=1,kmxs),
       .                       ((radius(i,j,k),i=1,imxs),k=1,kmxs),
       .                       (( theta(i,j,k),i=1,imxs),k=1,kmxs)
                      READ(iunit) num_bytes_read
                      IF (num_bytes .NE. num_bytes_read) THEN
                              WRITE(*,*)'Error: Reading VStage grid file data'
                              STOP
                      END IF
  50          CONTINUE
```

where i is the axial direction, j is the radial direction, and k is the transverse direction. The variables "num_bytes" and "num_bytes_read" are used to ensure the data is read correctly. If the two values do not match, then an error has occurred.

The flowfield solution files are formatted in blocks of data as well. Each file contains a list of the flow variables: pressure, density, density times axial velocity, density times radial velocity, density times transverse velocity, density times energy, an unknown variable, k turbulence variable, and ε turbulence variable. From these variables, all other flow values can be found.

Appendix E: Tecplot File Information

An example of the Tecplot header information format is given below:

```
TITLE = "Slice Data"
 VARIABLES = "X"
 "Y"
 "Z"
 "radius"
 "theta"
 "rho"
 "U"
 "rho*U"
 "V"
 "rho*V"
 "W"
 "rho*W"
 "Vmag"
 "Pressure"
 "Total Pressure"
 "Temperature"
 "Total Temperature"
 "Mach Number"
 "Rel Mach Numberr"
 "Energy"
 "Vrad"
 "Vmerid"
 "Vtan"
 "Vtanr"
 "VrelTotal"
 "VD"
 "ds_cp"
 "rUdscp"
 "s"
 "s - normalized"
 "Pt Ratio"
 "Tt Ratio"
 "efficiency"
 "span"
 ZONE T="Slice Data"
 I=      189  J=        1  K=        81  ZONETYPE=Ordered
 DATAPACKING = BLOCK
 DT = (DOUBLE DOUBLE DOUBLE DOUBLE DOUBLE DOUBLE DOUBLE
 DOUBLE DOUBLE DOUBLE DOUBLE DOUBLE DOUBLE DOUBLE DOUBLE
 DOUBLE DOUBLE DOUBLE DOUBLE DOUBLE DOUBLE DOUBLE DOUBLE
 DOUBLE DOUBLE DOUBLE DOUBLE DOUBLE DOUBLE DOUBLE DOUBLE
 DOUBLE DOUBLE DOUBLE )
```

The title of the Tecplot frame is given, followed by a list of the variable names, then by

the title of the zone. The number of nodes in the I,J,K direction is given next, along with

the arrangement type. How the data is packaged is given, in this case block, followed by

the variable type for each variable named. After the header information, the first variable

is listed in block format, followed by the second variable, etc.

Vita

Mark Willis Davey

Candidate for the Degree of

Master of Science

Thesis: INFLUENCE OF AXIAL SPACING ON EFFICIENCY VERSUS SPAN FOR A TRANSONIC COMPRESSOR ROTOR STAGE

Major Field: Mechanical Engineering

Biographical:

Personal Data: Born in Rochester, New York on August 16, 1979, the son of Kenneth and Mary Davey

Education: Graduated from Greece Athena High School, Rochester, New York in June 1998. Received a Bachelor of Science degree in Aerospace Engineering from Oklahoma State University, Stillwater, Oklahoma in May 2002. Completed the requirements for the Master of Science degree with a major in Mechanical Engineering at Oklahoma State University in December 2004.

Experience: Employed by Crane Carrier Company as an Engineering Intern from May to August 1999. Employed by NASA Langley as a Guest Researcher from 2001 to 2003. Employed by Oklahoma State University as a Research Assistant and Teaching Assistant in the Department of Mechanical and Aerospace Engineering from 2003 to 2004.

Professional Memberships: American Society of Mechanical Engineers, American Institute of Aeronautics and Astronautics, American Indian Science and Engineering Society.